ORIGIN AND DISTRIBUTION OF SOME TRACE ELEMENTS IN METAMORPHOSED
Fe–Mn DEPOSITS, VAL FERRERA, EASTERN SWISS ALPS

JOËL BRUGGER[§]

Department of Earth Sciences, Monash University, Clayton, Victoria 3800, Australia

RETO GIERÉ

Department of Earth and Atmospheric Sciences, Purdue University, West Lafayette, Indiana 47907-1397, U.S.A.

ABSTRACT

Numerous small Fe–Mn deposits occur in Triassic marbles of the Middle Penninic Suretta, Starlera, and Schams nappes in Val Ferrera, eastern Swiss Alps. These deposits are characterized by high contents of Ba, Sb, As, V, Be, W, and rare-earth elements (*REE*), and most likely represent chemical sediments deposited around submarine springs, similar to some modern seafloor metalliferous sediments. Circulation of the hydrothermal fluid within the granite-bearing basement underlying the sedimentary rocks is inferred as the most likely mechanism for the derivation of the Be and W concentrated in the ores. The orebodies studied shared a similar Alpine metamorphic evolution, culminating with blueschist- to greenschist-facies conditions. The chemical and mineralogical composition of the ores strongly influenced the behavior of the minor constituents Ba, Sr, Sb, As, V, Be, W, and *REE*. During the main deformation (D_1), As and V, for example, were incorporated into hematite in Fe-rich ores, whereas in Mn-rich ores they were concentrated into accessory minerals growing in the main schistosity. These syn-D_1 minerals represent important sinks of trace elements released by recrystallization or breakdown of their primary hosts as a result of prograde metamorphism. Post-D_1 mobility of Ba, Sb, As, V, Be, *REE* and, in some cases, W is recorded by various mineral parageneses that either overgrow the S_1 schistosity or occur in several types of discordant veins. In addition to the chemical and mineralogical controls, the structural position of the deposit influenced the remobilization of trace elements. Element mobility during the Alpine greenschist-facies metamorphism within the Fe–Mn ores involved large-ion lithophile elements (Be, Sr, Ba), high-field-strength elements (Mo, W, Sb, As), and the light *REE*. The geochemical signature is analogous in many respects to the remobilization observed during subduction-related metamorphism and during metasomatism in the mantle.

Keywords: exhalative Fe–Mn ores, metamorphism, paragenetic evolution, geochemistry, rare-earth elements, Val Ferrera, Swiss Alps.

SOMMAIRE

Les marbres Triassiques des nappes de Suretta, Starlera et Schams dans le Val Ferrera (Pennique Moyen, secteur est des Alpes suisses) renferment de nombreux petits gîtes de Fe et Mn. Ces minerais sont caractérisés par de hautes teneurs en Ba, Sb, As, V, Be, W, et terres rares par rapport aux carbonates encaissants. Les minerais résultent probablement d'une précipitation chimique à proximité de sources hydrothermales sous-marines, comme certains sédiments métallifères océaniques actuels. L'enrichissement des minerais en Be et W est lié à la circulation des fluides hydrothermaux au sein du socle granitique sous-jacent. Tous les gîtes étudiés ont subi le même métamorphisme Alpin, culminant sous faciès schiste bleu ou schiste vert. La composition chimique et minéralogique des minerais influence le comportement des éléments mineurs Ba, Sr, Sb, As, V, Be, W, et terres rares. Durant la phase principale de déformation (D_1), les éléments traces tels que As et V sont incorporés dans l'hématite des minerais riches en Fe. Cependant, dans les minerais riches en Mn, ces mêmes éléments sont concentrés dans des minéraux accessoires tels que la médaïte, qui croissent au sein de la schistosité principale. Ces minéraux accessoires sont des hôtes importants d'éléments en traces libérés par la recristallisation ou la déstabilisation des minéraux primaires au cours du métamorphisme prograde. La déformation postérieure à D_1 est associée à une mobilité des éléments en traces tels que Ba, Sb, As, V, Be, les terres rares et, dans certains cas, W. Ce second épisode, probablement polyphasé, est caractérisé par des paragenèses minéralogiques différentes qui se greffent sur les minéraux de la schistosité principale, ou qui apparaissent en veines discordantes. En sus de la chimie et la minéralogie du protolithe, la position structurale du gîte influence la remobilisation des éléments en traces. La mobilité des éléments en traces au sein des minerais de Fe–Mn durant le métamorphisme Alpin sous conditions du faciès schiste-vert concerne

[§] *E-mail address*: joelb@mail.earth.monash.edu.au

tant les éléments lithophiles à gros rayon (Be, Sr, Ba), les éléments à fort potentiel ionique (Mo, W, Sb, As), que les terres rares légères. Cette signature géochimique est analogue à celle observée durant la métasomatose mantellique ou la métasomatose associée au métamorphisme en zone de subduction.

Mots-clés: minerais Fe–Mn exhalatifs, métamorphisme, évolution paragénétique, géochimie, terres rares, Val Ferrera, Alpes Suisses.

INTRODUCTION

Manganese deposits metamorphosed under low- to high-grade conditions have furnished a large number of unusual minerals containing Sb, As, V, Be, W, the light rare-earth elements (*LREE*), Ba, and Sr. For example, minerals of Sb, As, and V have been observed, locally in relatively large quantities, in *radiolarite-hosted* deposits at Falotta in the Oberhalbstein, Switzerland (Geiger 1948), at Praborna in the Aosta Valley, Italy (Martin-Vernizzi 1984, Perseil 1991), and in the Ligurian Alps, Italy (Cortesogno *et al.* 1979), in other *chert-hosted* deposits in the Hautes-Pyrénées in France (Ragu 1990, 1994) and at Madhya Pradesh, India (Ostwald & Nayak 1993), in s*andstone-hosted* deposits at the Kombat mine, Namibia (Dunn 1991); and in *carbonate-hosted* deposits at Franklin, New Jersey, (Dunn 1995) and in Sweden and Norway (Långban-type deposits, Boström *et al.* 1979, Holtstam *et al.* 1998). Beryllium minerals, on the other hand, are reported from Långban (Sweden), Hautes-Pyrénées, Franklin (Essene & Peacor 1987), and Falotta (Graeser 1995), whereas W and *LREE* minerals were found at Långban, Hautes-Pyrénées, and Franklin. Finally, Ba and Sr minerals (mostly strontian barite) are present in all of the deposits mentioned above. A syngenetic exhalative origin has been inferred for all of these deposits. The timing of the enrichment in Sb, As, V, Be, W, *LREE*, Ba, and Sr, however, is not always clear because the minerals incorporating these elements occur mostly in late veins that postdate the peak of metamorphism.

Arsenic is typically enriched in synsedimentary Fe–Mn deposits (Pfeifer *et al.* 1988). Beryllium and W, on the other hand, are commonly associated with granitic rocks (Guilbert & Park 1986), and their occurrence in late veins within syngenetic Fe–Mn deposits has in some cases been interpreted as indicating chemical input from post-ore granitic intrusions (*e.g.,* Ragu 1990, 1994). In general, very little is known about the mobilization history of Sb, As, V, Be, W, *REE*, Ba, and Sr within metamorphosed Fe–Mn deposits in the time span between metamorphic climax and formation of the late veins, because geochemical studies aim to reconstitute the premetamorphic state, and mineralogical studies are mostly concerned with crystal–chemical features of the rare minerals rather than with genetic aspects.

We describe in this paper mineral assemblages recently discovered in four genetically related carbonate-hosted stratiform metamorphosed Fe–Mn deposits in Val Ferrera, eastern Central Alps, Switzerland. We present whole-rock geochemical data for these deposits, and discuss their genesis as well as the mechanisms responsible for the geochemical and mineralogical signatures. The deposits chosen for study are unusual because here, contrary to many other metamorphosed Mn deposits, the phases incorporating Sb, As, V, Be, W, the *LREE*, Ba, and Sr commonly occur as *rock-forming* minerals. This situation offers an opportunity to recognize textural relationships among the various minerals, and thus, to follow paragenetic evolution through time. Furthermore, small differences in geochemical composition and structural position of the deposits allow study of the influence of these parameters on the redistribution of trace elements during metamorphism.

REGIONAL GEOLOGY

Val Ferrera, a high valley with the source of a tributary to the Rhine in Graubünden (Switzerland), belongs geologically to the Middle Penninic domain (Briançonnais) of the Eastern Swiss Alps, which is characterized by shallow-water sedimentation from Triassic to Middle Jurassic (Trümpy 1980). In Val Ferrera, the Briançonnais platform was segmented into four distinct tectonic units during the Alpine orogeny: (1) the Tambo nappe, (2) the Suretta nappe, (3) the Starlera nappe, and (4) the Schams nappes (Baudin *et al.* 1995, Schmid *et al.* 1997; see Fig. 1). The Starlera and Schams nappes are sedimentary units that are disconnected from their basement, whereas the Suretta and Tambo nappes consist of a pre-Alpine basement underlying a thin sedimentary cover. This pre-Alpine basement comprises two main units, the Timun complex and the "Roffnaporphyr". The latter represents a large volume of Early Permian (268.3 ± 0.6 Ma; Marquer *et al.* 1998) volcanic to subvolcanic rocks of granitic composition, which underwent a single episode of metamorphism during the Tertiary. The Timun complex, on the other hand, is a polymetamorphic unit that consists of para- and orthogneisses and amphibolites. The Timun complex was subjected to a pre-Alpine eclogite- and amphibolite-facies metamorphism that was overprinted by Tertiary Alpine metamorphism (Nussbaum *et al.* 1998). The Suretta cover (Fig. 2) consists of locally preserved Permian clastic metasedimentary rocks followed by a basal quartzite (Permo-Triassic), and then by Triassic dolomitic marbles. This series is cut by rift structures filled with mono- and polygenetic breccias containing clasts of dolomite, quartzite, augen gneiss and, in places, hematite–quartz pebbles. All authors agree on a Mesozoic
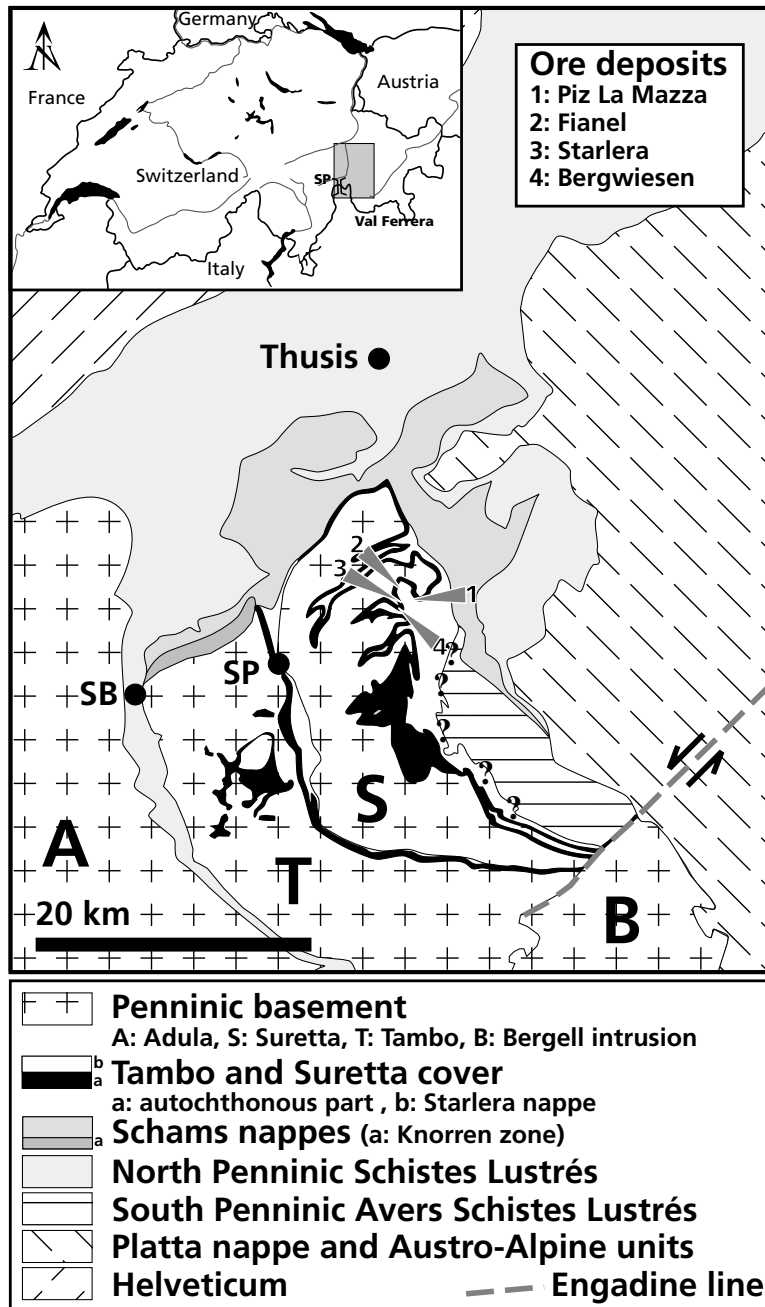
FIG. 1.   Tectonic map of the eastern Central Alps around Val Ferrera, Graubünden, Switzerland. Abbreviations: SB: San Bernardino, SP: Splügenpass. A "?" indicates where the contact between Avers Schistes Lustrés and the Suretta cover is uncertain.

synsedimentary origin of these breccias, although their precise age remains controversial (Liassic to Cretaceous; Baudin *et al.* 1995, Schmid *et al.* 1997). The series then grades into marbles and calc-schists, which are not distinguishable from those of the structurally higher tectonic unit, the South Penninic Avers Schistes Lustrés (Figs. 1, 2). The covers of the Suretta and the Starlera nappes are stratigraphically similar, but the Starlera cover is thicker, and the basal quartzite is generally missing.

Décollement and stacking of the Suretta, Starlera and Schams nappes predate the Tertiary metamorphism and thus, all of these units and the related ore deposits underwent a similar Tertiary metamorphic evolution. Four phases of deformation are distinguished (Schreurs 1995, Marquer *et al.* 1996, Schmid *et al.* 1997). D_1 (Ferrera phase) is a complex event, which started under blueschist-facies conditions estimated at 10 kbar and 400–450°C (Goffé & Oberhänsli 1992, Nussbaum *et al.* 1998). The main D_1 structures, however, developed under greenschist-facies conditions, and consist of large-scale isoclinal folds and a pervasive schistosity (S_1) that destroyed most earlier textures and paragenenses. The presence of stilpnomelane in the S_1 schistosity suggests an upper temperature limit of about 450°C (Nitsch 1970). The age bracket 35–40 Ma is the most realistic estimate of the timing of the temperature peak during D_1 (Hurford *et al.* 1989). The second phase of deformation D_2 (Niemet phase) occurred under greenschist-facies conditions and is, like D_1, associated with isoclinal folding; an axial-plane schistosity (S_2), however, developed only in the most incompetent rocks. By using the phengite geobarometer of Massonne & Schreyer (1987), Baudin & Marquer (1993) inferred that a decompression of at least 5 kbar took place between D_1 and D_2. The Bergell granodiorite, dated at 30.13 ± 0.17 Ma (von Blanckenburg 1992), cuts D_2 structures, and therefore sets a minimum age for D_2 (Liniger 1992). D_3 produced a fine crenulation in the most incompetent rocks, and the last event (D_4), occurring under brittle
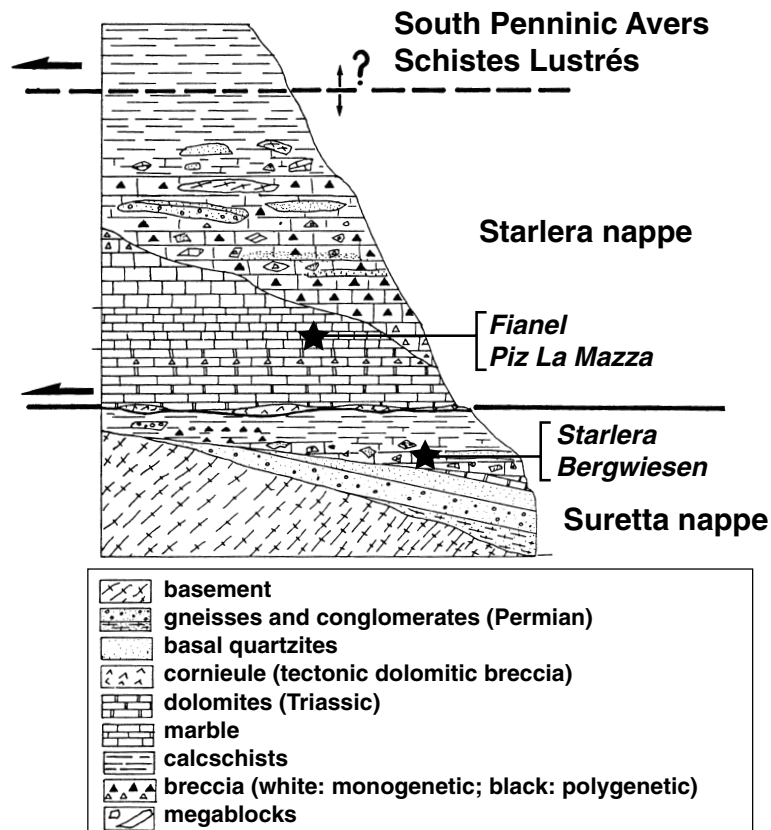

FIG. 2.   Schematic synthesis of a stratigraphic profile of the Suretta nappe cover showing the location of the deposits studied; modified after Baudin *et al.* (1995). Fe–Mn deposit names shown in italics.

conditions, was responsible for the formation of sub-vertical N–S-striking faults.

Two kinds of Fe–Mn deposits, both affected by the metamorphism associated with D_1, can be distinguished in Val Ferrera: (i) Fe-carbonate veins in the augen gneiss of the Timun complex (Suretta nappe; Grünenfelder 1956), and (ii) carbonate-hosted stratiform Fe–Mn deposits in the Triassic dolomite marbles of the Suretta, Starlera, and Schams nappes (Stucky 1960). The Fe-carbonate veins display a monotonous mineralogical composition consisting of siderite, ankerite, quartz ± stilpnomelane. Locally, "skarns" with aegirine, hematite or magnetite developed at the contact between the Fe-carbonate veins and the augen gneiss. The second type of ore is the focus of this study.

MINERALOGY OF THE CARBONATE-HOSTED STRATIFORM Fe–Mn DEPOSITS

The most common ores consist of hematite, quartz, and carbonate (dolomite), with strontian barite and fluorapatite as widespread minor constituents. Depending on the hematite:quartz ratio, the ores have a schistose or massive appearance. Significant amounts of Mn minerals are restricted to the largest deposits (Stucky 1960). All Mn deposits and some of the stratiform Fe deposits contain a range of unusual Sb, As, V, Be, W, Ba, Sr, and *REE* minerals (listed with their formula in Table 1). In this paper, however, we restrict our description to four deposits, in which the minerals mentioned reveal a paragenetic evolution or appear in special structural settings. The location of these deposits is indicated on Figure 1, and their tectonic and stratigraphic settings

TABLE 1. CHEMICAL FORMULAE OF THE Sb–As–V–Be–W–*REE*–Ba (Sr) MINERALS OBSERVED IN THE VAL FERRERA DEPOSITS

Name	Formula
Barite (strontian) [Brt]	$(Ba,Sr)SO_4$
Barylite [Blt]	$BaBe_2Si_2O_7$
Bergslagite	$CaBeAsO_4(OH)$
Beryl	$Be_3Al_2Si_6O_{18}$
Betafite	$(Ca,U,\square)(Ti,Nb,Ta)_2(O,OH)_7$
Chernovite-(Y)	$YAsO_4$
Fianelite	$Mn_2V(V,As)O_7 \cdot 2H_2O$
Långbanite	$(Mn^{2+},Ca)_4(Mn^{3+},Fe^{3+})_9Sb^{5+}O_{16}(SiO_4)_2$
Medaite [Med]	$(Mn,Ca)_6(V,As)Si_5O_{18}(OH)$
Palenzonaite	$NaCa_2Mn_2(VO_4)_3$
Paraniite-(Y)	$YAsO_4 \cdot 2CaWO_4$
Phenakite	Be_2SiO_4
Pyrobelonite	$PbMnVO_4(OH)$
Romanèchite	$(Ba,H_2O)_2Mn_5O_{10}$
Roméite	$(Ca,Na,\square)_2(Sb,Ti)_2O_6(F,OH,O)$
Saneroite	$Na_2Mn_{10}VSi_{11}O_{34}(OH)_4$
Scheelite–powellite	$CaWO_4 – CaMoO_4$
Tilasite	$CaMgAsO_4F$

The symbols are shown in square brackets. Other symbols used in tables and in figures are: Ae aegirine, Ank ankerite, Ap fluorapatite, Brn braunite, Cal calcite, Cdt calderite, Dol dolomite, Hem hematite, Kth kutnohorite, Mgt magnetite, Ms muscovite, Qtz quartz, Rds rhodochrosite, Rdn rhodonite, Sd siderite, Tep tephroite, and Tlc talc.

are shown in Figure 2. The methods of investigation are described in the Appendix.

Fianel

The Fianel deposit is hosted by dolomitic marbles of the Starlera nappe, with no apparent connection to the basal quartzite. Fianel is the largest deposit of hematite exploited in the past in Val Ferrera. The ores show a strong bedding (1 cm to 50 cm), with single beds exhibiting a lenticular shape (Fig. 3a). Fianel also contains Mn ores, which consist principally of silicate–oxide Fe–Mn ores (below referred to as "mixed ores") containing quartz, rhodonite, spessartine and andradite–calderite garnet, tephroite, rhodochrosite and kutnohorite, aegirine, hematite, braunite, jacobsite, barylite, and strontian barite. The mixed ores are very fine grained, and exhibit complex relationships among the different phases. For example, Figure 4 shows tephroite replacing rhodonite and rhodochrosite as a result of the reaction $Rdn + Rds = Tep + CO_{2(g)}$. In the same thin section, replacement of tephroite by calderite has been observed (see Table 2 for compositions of calderite, rhodonite and tephroite).

V–As minerals are very abundant at Fianel. The most spectacular samples consist of mixed ores, which exhibit a red color due to the presence of the vanadatosilicate medaite (Fig. 3b, Table 2). Medaite, $(Mn,Ca)_6(V,As)Si_5O_{19}(OH)$, was described by Gramaccioli *et al.* (1982) in the low-grade metamorphosed, radiolarite-hosted Mn deposits of Val Graveglia, Italy. To the best of our knowledge, Fianel is only the second reported occurrence of this mineral. In contrast to the type locality, where medaite is a rare constituent of discordant veinlets, medaite at Fianel represents up to 3 vol.% of the rock and is aligned in the main S_1 schistosity (Figs. 3b, d). A further rock-forming V-rich mineral is an unidentified V–Ba–Sr phase (±As, Fe, Mn, Pb) that forms xenomorphic crystals up to 10 μm in diameter. The Mn ores are cut by several generations of veinlets consisting of quartz, rhodonite, rhodochrosite ± aegirine, andradite–calderite garnet, parsettensite, and strontian barite. Where occurring in medaite-rich ores, these veinlets also contain the vanadates palenzonaite, saneroite, and pyrobelonite (*cf.* Table 1, Fig. 3c). A hydrated Mn vanadate, fianelite, has been discovered in open fractures cutting such veinlets (Brugger & Berlepsch 1996).

In a V-rich mixed ore, we observed one grain of a mineral that is tentatively identified as långbanite on the basis of electron-microprobe data (Table 3); no other method of identification was used in order to preserve this unique grain. Långbanite has been reported from small Långban-type Mn deposits in the Långban and Sjögruvan provinces, Sweden, and at Brandsnuten, Norway (Nysten & Ericsson 1994). The chemical composition of långbanite from Fianel is very similar to that of the Fe-rich långbanite from the Nyberget deposit in Sjögruvan Province (Table 3). At Fianel, the långbanite

FIG. 3. Petrography of sediment-hosted stratiform Fe–Mn ores in Val Ferrera. (a) Outcrop of hematite–quartz ore at Fianel, showing lenticular bedding. (b) Outcrop of medaite-rich (orange vanadatosilicate) mixed Fe–Mn silicate–oxide ore at Fianel. (c) Mn ore (dark: mainly braunite; light: mainly rhodonite + rhodochrosite, cross-cut by veinlets consisting of quartz + rhodochrosite + palenzonaite (Bordeaux red) at Fianel. (d, e) Microphotographs of the medaite-bearing Fe–Mn mixed ores from Fianel; (d) in transmitted light with parallel polarizers, and (e) under cathodoluminescence. (f) Hematite – kutnohorite – fluorapatite schist from Bergwiesen (JB131), with two clasts of manganoan calcite (*).

FIG. 4.   BSE image of a mixed ore from Fianel, showing a grain of rhodonite undergoing transformation to tephroite.
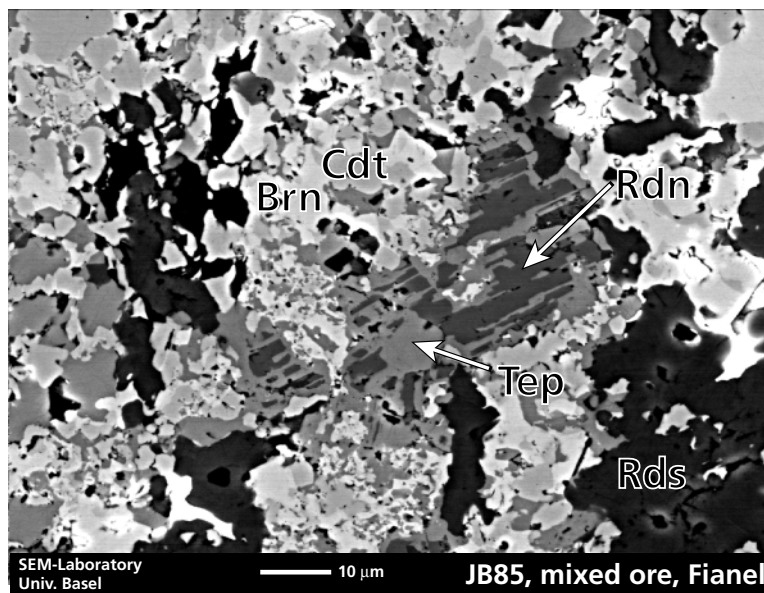
TABLE 2. CHEMICAL COMPOSITION OF SOME ROCK-FORMING MINERALS
IN THE CARBONATE-HOSTED Fe–Mn ORES AT VAL FERRERA

Number	#1	#2	#3	#4	#5	#6	#7
Sample	JB85	JB85	JB325	JB314	JB131	JB131	JB131
Mineral	Tep	Rdn	Cdt	Med	Sps	Cal	Kth
Average of	10	6	2	11	30	7	6
SiO_2 wt%	30.35 (1.49)	49.41 (0.33)	34.22	37.84 (0.44)	36.26 (1.13)		
TiO_2			0.06		0.15 (0.15)		
Al_2O_3	<0.03		4.54		17.09 (3.43)		
V_2O_5	0.06 (0.05)	0.07 (0.04)		7.32 (0.59)	0.07 (0.06)		
As_2O_5	<0.05	<0.05		1.82 (0.51)			
Fe_2O_3			22.92		5.03 (4.31)		
FeO	0.13 (0.12)	<0.05		1.79 (0.31)		<0.17 (0.22)	<0.17 (0.22)
CaO	0.12 (0.07)	2.03 (0.33)	11.32	0.45 (0.04)	4.53 (1.62)	37.10 (1.39)	27.86 (1.96)
MgO	2.58 (1.58)	2.70 (0.23)	0.04	0.73 (0.03)	0.09 (0.04)	0.85 (0.41)	1.66 (0.16)
MnO	66.65 (1.93)	47.78 (0.89)	28.53	48.91 (0.27)	36.19 (1.02)	17.73 (1.95)	26.49 (1.65)
SrO						0.17 (0.13)	0.03 (0.03)
CO_2 (calc.)						41.11	40.22
H_2O (calc.)				1.10			
Sum	99.93	102.0	101.63	99.96	99.41	96.95	96.43

Structural formulae:
#1 $Si_{1.00}(Mn_{1.86}Mg_{0.14})O_4$ (normalization on 3 cations)
#2 $Si_{1.03}(Mn_{0.84}Mg_{0.08}Ca_{0.05})O_3$ (normalization on 2 cations)
#3 $Si_{2.94}(Fe^{3+}_{1.48}Al_{0.46})(Mn^{2+}_{2.07}Ca_{1.04})O_{11.9} = Cdt_{41}Adr_{36}Sps_{23}$ (normalization according to Rickwood 1968)
#4 $Si_{5.0}(V_{0.66}Si_{0.15}As_{0.13})(Mn_{5.64}Fe_{0.20}Mg_{0.15})HO_{18.8}$ (normalization on 12 cations)
#5 $Si_{3.02}(Al_{1.68}Fe_{0.32}Ti_{0.01})(Mn_{2.55}Ca_{0.40}Mg_{0.01})O_{12.02}$ (normalization on 8 cations, $Fe^{3+} = Fe_{tot}$, $Mn^{2+} = Mn_{tot}$)
#6 $(Ca_{0.71}Mn_{0.27}Mg_{0.02})CO_3$
#7 $(Ca_{0.54}Mn_{0.41}Mg_{0.05})CO_3$

The standard deviation (1σ) associated with the electron-microprobe data is shown in parentheses. JB85, JB314, and JB325 are mixed ores from Fianel; JB131 is a fluorapatite – kutnohorite – hematite schist from Bergwiesen.

TABLE 3. COMPOSITION OF LÅNGBANITE
(ELECTRON-MICROPROBE DATA)

	Fianel #1	σ_{n-1}	Nyberget #2		Fianel #1		Nyberget #2
SiO₂ wt%	9.95	0.15	9.06	[8]Mn³⁺	0.962	0.02	0.898
Sb₂O₅	12.03	0.21	13.39	[8]Ca	0.038	0.01	0.102
As₂O₅	0.27	0.11	n.a.	Σ[8]	1.000		1.000
TiO₂	1.00	0.17	0.19				
Fe₂O₃	18.73	0.17	18.97	[6]Mn³⁺	3.599	0.09	3.729
MnO	23.31	0.36	21.01	[6]Fe³⁺	2.983	0.03	3.111
Mn₂O₃	34.52		35.08	[6]Mn²⁺	4.178	0.06	4.072
CaO	0.17	0.04	0.44	[6]Sb⁵⁺	0.135	0.04	0.114
				Σ[6]	10.895	0.03	11.025
Sum	99.98		98.14				
				[6]Sb⁵⁺	0.811	0.03	0.970
				[6]As⁵⁺	0.030	0.01	
				[6]Ti⁴⁺	0.159	0.03	0.030
				Σ[6]	1.000		1.000
				[3]Mn³⁺	1.000		1.000
				[4]Si	2.11	0.03	1.970
				O	24.00		24.00

Column 1: långbanite (?), mean and standard deviation of nine determinations (electron-microprobe data), sample JB31. Column 2: långbanite from Nyberget, Sweden (Nysten & Ericsson 1994). The Y content reported by Moore *et al.* (1991) is most likely due to the interference between YLα and ²SbLβ (Nysten & Ericsson 1994), and thus was omitted. The compositions are normalized to 16 cations, Fe_{total} = Fe^{3+}, Σ[8] = 1. and the Mn^{2+}:Mn^{3+} ratio was calculated to obtain 24 atoms of oxygen per formula unit.

grain contains a sigmoidal internal fabric that is defined by quartz, and oriented discordantly to the D_1 foliation of the surrounding matrix (Fig. 5). The entire grain is cut by a conjugate set of narrow shears. The inner foliation in långbanite likely represents a premetamorphic feature, and the långbanite thus probably grew synkinematically with respect to D_1.

Barylite, $BaBe_2Si_2O_7$, is a common accessory mineral within the S_1 schistosity of the medaite-rich mixed ores (Figs. 3d, e). Beryl occurs at Fianel in two varieties, as anhedral blue grains in discordant quartz veins within hematite – quartz – carbonate ores (type I), and as euhedral crystals in a lens of pink dolomite breccia (type II). Phenakite occurs in some of the pink dolomite clasts. Type-II beryl is associated with As- and *REE*-rich scheelite–powellite, roméite, bergslagite, and fluorapatite in discordant quartz–dolomite veinlets; during a later stage of metamorphism, these veinlets were infiltrated by a fluid that led to partial replacement of the original grains of fluorapatite by As-rich fluorapatite, and to the appearance of paraniite-(Y) in scheelite–powellite (Brugger *et al.* 1998).

Piz La Mazza

A hematite – quartz – carbonate – fluorapatite – strontian barite schist, up to 1 m thick, crops out at Piz

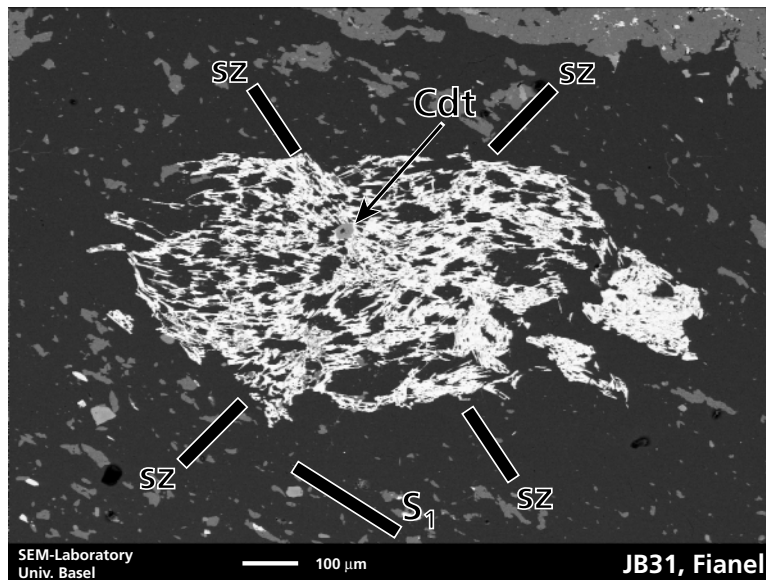

FIG. 5. BSE image of a långbanite (?) grain from Fianel, Val Ferrera. Abbreviations: sz: shear zone, S_1: main schistosity. The matrix contains quartz (dark gray), and a complex assemblage of Fe–Mn silicates, carbonates, and oxides (rhodonite, spessartine and andradite–calderite garnet, tephroite, rhodochrosite and kutnohorite, aegirine, hematite, braunite, jacobsite, and strontian barite).

La Mazza (Starlera nappe). As at Fianel, the deposit does not seem to have a direct connection to the basal quartzite. The hematite schist at Piz La Mazza contains spherulitic muscovite that encloses hematite, fluorapatite and, rarely, an yttrium phosphate mineral [xenotime-(Y), or possibly churchite-(Y)], and which is locally finely intergrown with carbonate (Fig. 6a). Fluorapatite is also present in the S_1 schistosity and may further be concentrated along the margin of the spherules (Fig. 6a). Hematite generally defines S_1, but some spherules con-
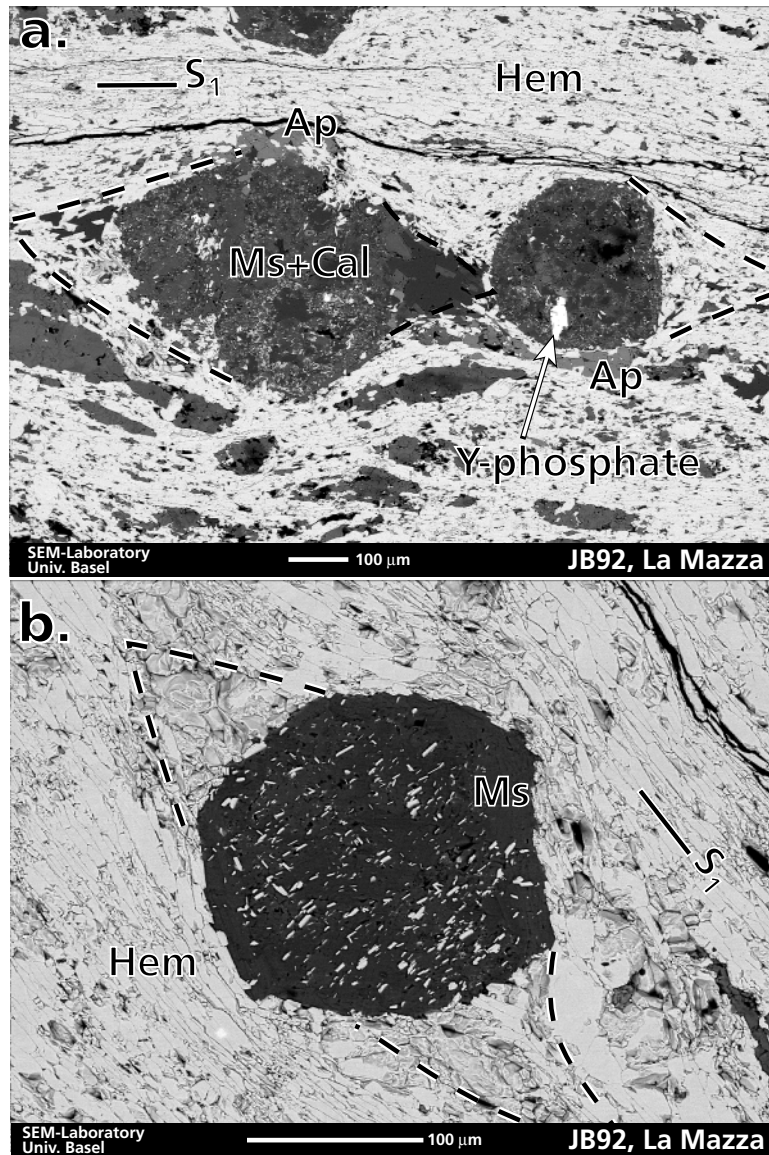
FIG. 6. BSE images of muscovite spherules from Piz La Mazza, Val Ferrera. Dashed lines delineate the pressure shadows of the spherules. (a) Spherule consisting of muscovite and calcite. Note the yttrium phosphate inclusion [possibly xenotime-(Y)] and the concentration of fluorapatite along the rim; hematite is the predominant mineral in the main schistosity S_1; (b) Muscovite spherule with oriented inclusions of hematite. Note that the orientation of the hematite within the spherule is discordant to S_1.

tain trails of small crystals of hematite oriented discordantly to S_1 (Fig. 6b). The S_1 schistosity wraps around the spherules, and a pressure shadow consisting of quartz + hematite is commonly observed (Figs. 6a, b). These features clearly indicate a pre-D_1 timing for the formation of the spherules.

Bergwiesen

The Bergwiesen deposit (Suretta nappe) is a small hematite-rich orebody (up to 2 m thick) that can be followed continuously over 70 m. The concordant nature of the orebody and many examples of fine lamination are well preserved. Although the mineralogy of Bergwiesen contrasts with that of the Starlera deposit (located about 200 m away), both deposits are contained in dolomitic marbles just above the contact with the basal quartzite, and probably lie in stratigraphic continuity (Fig. 7).

Besides Fianel, Bergwiesen is the only deposit were beryl was identified. Here, the mineral occurs, like type-I beryl at Fianel, as anhedral grains up to 1 cm across in discordant quartz veins associated with minor hematite and rare chalcopyrite.

Ores containing up to 10.60 wt% P_2O_5 are characteristic of Bergwiesen. There ores are strongly foliated and banded, with alternating hematite and carbonate + fluorapatite-rich layers (Fig. 3f). The hematite-rich layers contain some clasts of Mn-rich calcite (Fig. 3f), but the main carbonate is kutnohorite (Table 2). Kutnohorite and fluorapatite, together with hematite, quartz, muscovite, and minor strontian barite, define the S_1 schistosity. In addition to these minerals, spessartine porphyroblasts with a diameter of up to 0.5 mm are abundant. Under the optical microscope, the spessartine crystals seem cloudy owing to the presence of many minute inclusions of fluorapatite. As revealed by back-scattered electron (BSE) images, these inclusions are either randomly distributed (Fig. 8a), or arranged in trails together with kutnohorite, quartz, and hematite (Fig. 8b). The inclusion trails define a schistosity that is commonly discor-

dant to S_1 and, in some cases, sigmoidal in shape (Fig. 8b). Most spessartine porphyroblasts have an inclusion-free, optically clear outer fringe (Fig. 8a). The fluorapatite inclusions are angular and completely surrounded by a fine network of spessartine (Fig. 8c); in some cases, the inclusions occupy a volume that is larger than that of the host garnet (Fig. 8d). The size of the apatite inclusions (≤ 5 μm) in the spessartine grains contrasts with that of the fluorapatite crystals (up to 40 μm) that occur outside the porphyroblasts, aligned in S_1 (Fig. 8).

The trails of inclusions likely represent a relic of the premetamorphic fine banding of the ore: the small crystals are preserved as inclusions within the garnet, whereas the premetamorphic minerals have recrystallized during D_1 into larger crystals that are present in the matrix surrounding the porphyroblasts.

The fluorapatite is chemically relatively homogeneous and contains, in addition to P, Ca, and F, 1.24 (± 0.06; standard deviation of seven analyses) wt% As_2O_5, 0.17 (± 0.04) wt% SrO, 0.09 (± 0.09) wt% FeO, and 0.39 (± 0.05) wt% MnO. Occurrence of nonstoichiometric F and P contents suggests that some phosphorus is replaced by carbon (Nathan 1996). No chemical difference was observed between the fluorapatite included in spessartine and that occurring in S_1.

Starlera

The Starlera mine (Suretta nappe) is the only deposit of the province that was exploited for Mn (from 1917 to 1920; Stucky 1960). This deposit is characterized by a complicated paleogeographic and structural position. The ore is hosted in dolomitic marbles, but may be in direct contact with the augen gneiss of the underlying basement (Fig. 7). In the vicinity of Starlera, the basal quartzite exhibits large variations in thickness, from >20 m at Bergwiesen to zero at Starlera. These variations in thickness might represent a Triassic paleogeography (trough) that favored ore deposition at Starlera. The present thickness of the ore, up to 12 m, also reflects doubling of the sequence by folding. Breccias with a matrix rich in magnesioriebeckite asbestos are abundant and characteristic of the Starlera deposit.

The Mn ores at Starlera are relatively poor in Si. Braunite is the main ore mineral, and the Mn-silicates rhodonite and spessartine are absent. Fine needles of romanèchite occur along braunite grain-boundaries. The ore is cut by numerous discordant roméite–tilasite veins. The latter are up to 30 cm thick, and display an uncommon mineral assemblage consisting of octahedra of fluorian roméite (≤ 5 mm), coarse-grained tilasite, idiomorphic aegirine, calcite, hydroxyl-phlogopite, and fluorite (Brugger *et al.* 1997).

Tilasite is also present in some hematite – carbonate – quartz ores that are interbedded between Mn ores and country-rock carbonates. These ores exhibit a banded to lenticular texture. Greenish tilasite is the main constituent of some concordant bands and lenses (up to
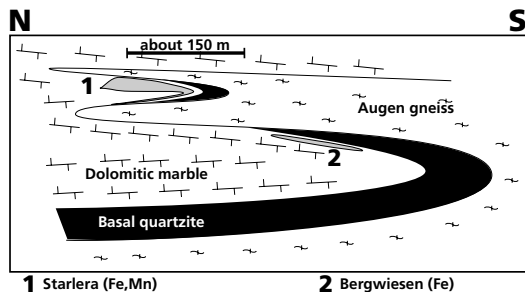
FIG. 7.   Schematic cross-section illustrating the tectonic setting of the Starlera and Bergwiesen deposits, Val Ferrera.
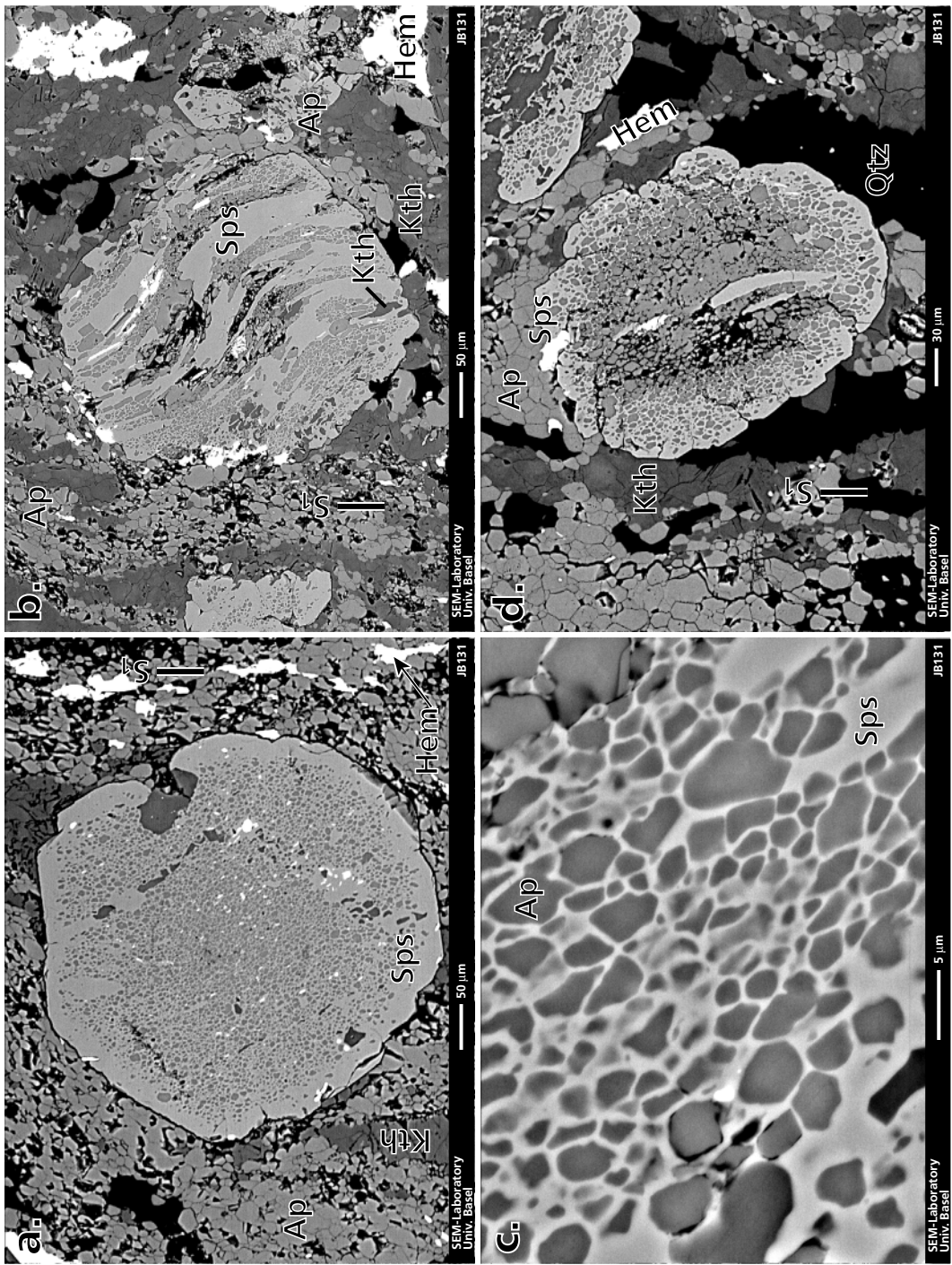
FIG. 8. BSE images of spessartine in the fluorapatite – kutnohorite – hematite schist from Bergwiesen, Val Ferrera. (a) Spessartine porphyroblast with randomly distributed inclusions of fluorapatite. (b) Spessartine porphyroblast with sigmoidal inclusion-trails of fluorapatite and kutnohorite. (c) Close-up view of fluorapatite inclusions in a spessartine host crystal. (d) Spessartine porphyroblast with a core dominated by fluorapatite inclusions. S_1 = main schistosity.

3 cm $\times$ 0.5 cm in size). Tilasite also occurs in discordant veinlets (<2 mm in thickness) in this hematite – carbonate – quartz ore.

A complex association of Ti, As, Sb, Be, Ba ($\pm$REE, W, Sr) minerals has been described by Brugger & Gieré (1999) from quartz-rich pink muscovite – aegirine – albite schists (hereafter referred to as "pink schists") interbedded with the Fe–Mn ores. Aligned in the main S_1 schistosity are strontian barite, As-poor fluorapatite, Sb-free rutile, and possibly Ce-rich roméite and Sb-bearing pyrophanite. A later paragenesis, overgrowing S_1, contains As-rich fluorapatite, REE-rich roméite, bergslagite, Sb-rich rutile, Sb-bearing pyrophanite, and Sb–As-bearing titanite, as well as aegirine porphyroblasts. Arsenic-rich fluorapatite, bergslagite, stibian rutile, and stibian pyrophanite occur in fractures within titanite crystals.

WHOLE-ROCK COMPOSITION OF THE ORES AND THEIR HOST ROCKS

The Fe/(Fe + Mn) values of the siderite veins are similar to those of their augen gneiss host-rock (Fig. 9a). In contrast, the carbonate-hosted deposits display a wide range of Fe/(Fe + Mn) values that range between 0 and 1 (Fig. 9b). Whole-rock geochemical data demonstrate that all carbonate-hosted stratiform ores of Val Ferrera are characterized by high concentrations of Sb, As, V, Be, and W relative to both the host rocks and Fe-carbonate veins (Tables 4, 5, Fig. 10).

The W and Be contents of the carbonate-hosted stratiform ores are higher that those of the Fe-carbonate veins and of the country rocks (Fig. 10a). The samples with high Be contents commonly also have high W contents. Two samples with unusual mineralogy do not follow this trend: JB423, which contains >10 vol.% roméite, a phase in which W is highly compatible, and JB101, which contains beryl and scheelite–powellite. In the V *versus* As diagram (Fig. 10b), there is a marked difference between mixed Fe–Mn ores from Fianel and the Fe ores: at high levels of trace-metal enrichment, the mixed ores generally exhibit a high V:As ratio, whereas this ratio is low for the Fe ores. Similarly, the roméite-rich ore JB423 and one sample of Mn-ore (sample JB161) exhibit a high As:V ratio.

A Sr *versus* Ba variation diagram (Fig. 11) reveals that Sr contents of the carbonate-hosted Fe and Mn ores are similar to those of the Triassic marbles, but that the Ba contents are much higher in the ores. There is a distinct positive correlation between Sr and Ba in the carbonate-hosted ores, particularly in the mixed Fe–Mn ores from Fianel. The Fe-carbonate veins, on the other hand, are relatively poor in Ba and Sr. Compared to their host rocks, the veins have similar Sr, but lower Ba contents (~300 ppm in the augen gneiss; Balzer 1989).

Chondrite-normalized REE patterns of the Fe-carbonate veins in the basement rocks are relatively flat, but exhibit a distinct positive Eu anomaly; these patterns are in marked contrast to the pattern of the augen gneiss, characterized by enrichment in LREE relative to heavy REE (HREE) and by a negative Eu anomaly (Fig. 12a). The REE patterns of the carbonate-hosted ores (Fig. 12b) display a greater complexity. (i) Most of the Fe ores have relatively flat REE patterns, exhibiting a wide range of Eu anomalies [Eu/Eu* = 2 $Eu_{CN}/(Sm_{CN} + Gd_{CN})$] from < 0.1 to 1.32, and a slightly negative Ce anomaly [Ce/Ce* = 2 $Ce_{CN}/(La_{CN} + Pr_{CN})$ = 0.92 to 0.47]. (ii) The Fe-rich ore JB306 has an LREE-enriched pattern, which is relatively parallel to that of the Triassic marbles. The pink ferroan dolomite from the beryl-bearing breccia at Fianel has a similar REE pattern. (iii) Most Mn-rich ores have REE contents intermediate between those of the Fe ores and carbonate host-rocks, but they all display negative Eu anomalies (Eu/Eu* between <0.1 and 0.7); Ce anomalies range between negative and positive values (Ce/Ce* in the range 0.05–1.99).

DISCUSSION

Genesis of the Fe-carbonate veins

The abundance of Fe-carbonates in late (D_4?) Alpine vugs within the augen gneiss illustrates the ability of
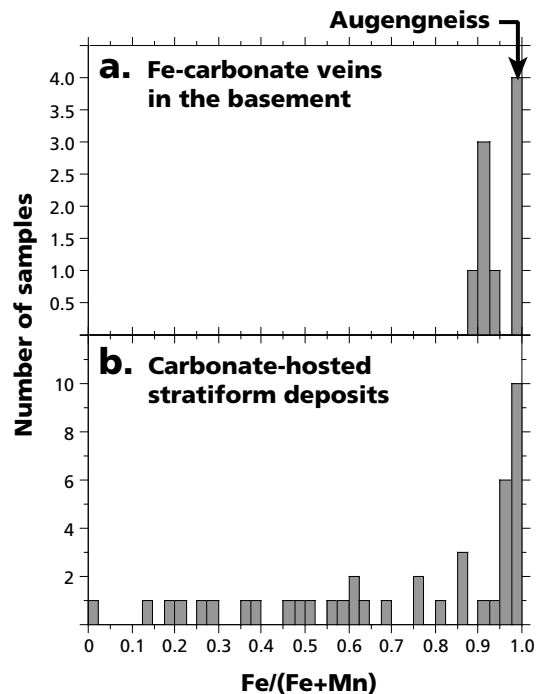

FIG. 9. Distribution of the Fe/(Fe + Mn) values in the ores from Val Ferrera, showing the contrast between the Fe-carbonate veins in the basement (a) and the carbonate-hosted mineralization (b).

TABLE 4. WHOLE-ROCK COMPOSITIONS OF THE ORES OF VAL FERRERA

	JB 174	JB 175	JB 120	JB 160	JB 122	JB 124	JB 156	JB 131	JB 133	JB 100	JB 101	JB 105	JB 147	JB 166	JB 302	JB 320(†)	JB 306	JB 92	JB 337.1	JB 407	JB 423
SiO₂	1.64	4.74	44.91	85.09	56.29	21.48	18.75	7.30	20.19	61.99	46.47	56.02	32.85	48.68	49.48	3.52	1.41	6.30	6.75	5.72	1.36
TiO₂	0.07	<0.02	0.06	<0.02	0.02	<0.02	0.04	0.05	<0.02	<0.02	0.05	0.02	0.02	0.02	0.04	<0.03	0.09	0.03	0.03	0.03	0.10
Al₂O₃	0.29	0.04	2.41	1.06	1.28	0.96	1.93	1.29	0.06	0.27	1.22	0.58	0.26	0.23	1.57	0.32	0.09	0.58	0.42	0.37	0.39
Fe₂O₃	0.73	0.11	47.05	13.58	22.25	39.33	42.98	23.87	70.50	37.14	32.68	40.01	45.10	5.80	21.30	0.56	87.29	77.83	31.09	32.60	2.61
MnO	0.21	0.31	0.12	0.01	1.69	4.40	3.04	13.59	2.15	0.12	0.51	0.13	12.85	34.25	2.85	0.95	2.41	3.56	27.38	22.03	4.17
MgO	7.06	0.26	0.26	0.01	1.74	3.02	4.04	0.88	0.27	0.01	4.80	0.79	0.23	0.55	3.35	19.56	0.26	0.87	3.56	2.87	5.75
CaO	44.90	47.16	1.09	0.04	2.37	5.73	2.89	22.26	3.03	0.19	5.10	0.86	1.35	1.04	7.47	24.72	4.87	3.96	10.13	14.97	25.99
Na₂O	<0.05	<0.05	2.40	0.48	<0.05	<0.05	<0.05	<0.05	<0.05	<0.05	<0.05	<0.05	0.60	0.39	6.40	<0.05	<0.05	<0.05	0.12	0.11	1.07
K₂O	0.15	<0.03	0.76	0.16	0.36	0.45	0.88	0.15	0.05	0.11	0.62	0.28	0.03	0.01	0.13	0.10	<0.03	0.16	0.38	0.39	0.02
P₂O₅	0.03	<0.03	0.03	<0.03	<0.03	<0.03	<0.03	9.74	0.19	0.15	0.22	0.16	0.20	0.08	0.06	0.19	0.16	0.19	<0.03	0.18	1.78
LOI	42.93	40.10	0.57	0.25	13.99	24.25	25.67	12.39	3.20	0.07	7.69	1.15	2.48	0.95	4.86	44.99	3.17	4.86	16.61	15.63	27.54
CO₂	43.52	41.92	1.25	0.33	15.47	25.11	28.16	13.57	3.54	0.04	7.64	1.05	3.00	2.02	5.25	n.d.	3.60	4.70	18.30	17.54	28.70
Total	98.01	92.72	99.66	100.68	99.99	99.62	100.22	91.52	99.64	100.05	99.36	100.00	95.97	92.00	97.51	94.91	100.29	98.34	96.47	94.90	70.78
††	98.11	92.81	99.68	100.68	100.18	100.11	100.56	94.02	100.02	100.08	99.44	100.03	98.32	97.12	98.62	95.02	100.67	99.22	99.89	98.19	82.71
*As	45	11	<4	<4	<4	<4	<4	1130	75	69	123	92	783	531	448	4	1937	<4	5783	411	3617
*Ba	477	319	43	<8	<8	<8	12	5679	800	112	78	42	5261	7329	4650	21	527	2807	1716	4627	2104
Be	1.0	<0.2	<0.2	0.2	0.2	0.3	0.7	33.1	175.1	78.6	78.4	96.2	42.6	33.8	168	1.6	13.8	25.2	15.7	29.7	0.7
Bi	<0.1	0.1	0.3	0.1	<0.1	0.3	0.1	0.2	0.1	0.1	0.1	0.1	0.1	<0.1	0.2	0.2	0.3	0.6	<0.1	0.1	0.4
Cd	<0.1	0.4	<0.1	<0.1	0.1	<0.1	0.1	0.3	<0.1	<0.1	0.1	<0.1	0.6	0.2	0.4	0.2	<0.1	4.2	0.3	0.1	0.3
Co	<0.5	<0.5	<0.5	<0.5	1.5	3.4	3.7	13.7	11.2	<0.5	<0.5	<0.5	0.7	6.0	2.6	<0.5	14.7	2.0	<0.5	<0.5	8.1
Cr	<1	<1	<1	3.3	<1	<1	<1	5.3	3.8	3.9	7.4	9.1	10.8	0.8	7.2	2.8	6.6	2.4	2.4	<1	2.7
Cs	3.1	0.1	0.1	0.7	0.5	0.5	2.8	1.8	1.5	0.9	6.4	2.9	1.5	1.5	1.5	1.0	0.2	0.9	14.4	10.2	0.3
Cu	24	60	2	35	35	20	31	46	24	18	14	22	54	346	26	9	51	15	26	55	24
Ga	<1	<1	<1	<1	1.5	1.9	3.0	4.3	2.7	1.3	3.0	1.6	2.6	5.8	5.0	<1	1.5	3.7	4.5	3.8	2.1
Ge	0.5	0.1	0.9	5.3	3.1	1.5	1.1	28.7	8.8	6.6	10.0	7.5	13.6	14.3	28.1	0.8	0.5	2.0	13.2	12.6	1.5
Hf	<0.1	<0.1	0.1	0.1	0.2	0.4	0.5	0.5	<0.1	0.1	0.3	0.1	<0.1	<0.1	0.1	<0.1	0.1	0.1	0.1	0.1	0.1
In	<0.05	<0.05	0.18	0.08	0.90	1.63	1.85	<0.05	<0.05	<0.05	<0.05	<0.05	<0.05	<0.05	<0.05	<0.05	<0.05	<0.05	<0.05	<0.05	<0.05
Mo	0.8	5.1	<0.2	1.3	1.6	3.0	1.2	1.2	5.9	1.5	54.2	12.1	2.3	2.5	1.5	15.8	2.1	2.2	0.7	1.5	0.5
Nb	0.2	<0.2	0.2	0.5	0.6	0.8	1.7	0.6	0.2	0.3	1.1	0.5	0.2	0.6	0.4	0.8	1.3	0.6	0.3		8.2
Ni	13	11	1	7	9	10	11	71	50	23	16	18	130	212	352	19	84	30	562	262	90
Pb	44	21	4	33	4	7	11	34	19	7	34	26	88	56	409	33	15	39	23	16	60
Rb	9.8	<1	3.4	19.6	4	22.1	61.7	8.3	4.8	5.0	25.7	10.3	1.1	9.6	3.5	<1	8.2	23.9	20.0	3.0	
*Sb	<4	<4	<4	<4	<4	<4	<4	12	38	17	16	3	31	31	19	1	184	8	331	118	83507
Sc	22.9	23.0	4.1	0.7	3.6	7.0	5.5	16.4	5.8	2.2	6.4	3.1	4.6	4.2	7.3	19.7	8.0	7.4	10.3	13.2	16.9
Sn	1.4	0.7	<0.5	2.8	3.1	2.3	3.5	1.5	0.8	1.1	1.3	1.5	1.4	1.8	1.2	<0.5	3.7	1.6	1.8	3.7	2.6
*Sr	455	1228	6	<4	18	28	38	541	61	10	60	14	979	1496	394	177	175	134	434	723	2052
Ta	<0.1	<0.1	<0.1	0.1	0.1	0.1	0.2	<0.1	<0.1	<0.1	0.1	<0.1	<0.1	<0.1	<0.1	<0.1	<0.1	0.1	0.1	<0.1	0.2
Th	<0.5	<0.5	<0.5	<0.5	0.7	1.9	1.2	0.7	<0.5	<0.5	0.9	<0.5	<0.5	1.2	<0.5	2.2	0.5	<0.5	<0.5	0.8	
Tl	<0.5	<0.5	<0.5	<0.5	<0.5	<0.5	<0.5	<0.5	<0.5	<0.5	0.9	<0.5	<0.5	<0.5	<0.5	<0.5	<0.5	3.9	3.3	<0.5	
U	<0.5	0.7	<0.5	<0.5	<0.5	0.7	<0.5	<0.5	0.6	0.5	0.9	<0.5	1.6	10.3	<0.5	1.9	<0.5	1.4	2.4	0.6	30.2
*V	58	9	27	6	10	10	11	88	468	135	113	95	1711	872	200	52	11	447	717	77	8
W	0.4	0.1	0.1	1.4	0.5	0.5	1.4	6.9	26.0	14.3	81.4	29.0	13.2	3.9	52.9	21.2	7.5	18.8	8.8	11.8	61.1
Y	0.9	0.4	0.9	4.5	8.6	12.8	18.5	58.6	53.3	19.1	20.0	14.5	13.0	12.2	4.8	5.1	4.0	24.2	25.4	18.3	14.0
Zn	18.9	5.7	1.3	2.1	13.2	27.3	23.5	156	122	33.4	111	26.7	379	1290	915	65	54	49	1120	563	89
Zr	2.2	0.6	2.9	4.6	5.1	10.7	17.0	30.3	3.2	2.7	11.8	4.3	2.0	5.1	3.2	1.5	2.8	6.0	9.8	4.3	9.9
La	1.1	0.9	0.9	1.5	2.8	6.2	4.1	14.3	6.7	5.0	6.8	3.7	2.8	22.8	2.6	2.1	6.7	4.3	2.0	2.2	15.3
Ce	1.8	1.1	1.9	3.4	6.0	13.4	8.6	12.6	6.0	8.9	12.0	6.7	3.2	2.0	3.2	2.4	3.4	6.8	7.9	4.4	24.6
Pr	0.23	0.16	0.25	0.43	0.74	1.80	1.11	2.39	1.28	1.00	1.79	0.84	0.30	2.68	0.48	0.35	1.04	0.83	0.42	0.52	1.41
Nd	0.7	0.3	1.1	1.8	3.2	9.2	4.7	9.5	6.2	3.8	6.8	3.1	1.2	9.3	2.0	1.4	3.7	3.4	1.8	2.3	5.8
Sm	0.1	<0.1	0.4	0.6	1.4	3.5	2.2	2.1	1.6	0.9	1.6	0.6	0.2	1.5	0.4	0.3	0.4	0.6	0.4	0.5	1.4
Eu	<0.01	<0.01	0.23	0.46	1.31	2.81	2.38	0.54	0.71	0.43	0.58	0.29	<0.01	0.36	<0.01	0.07	0.09	<0.01	0.06	<0.01	0.19
Gd	0.10	<0.1	0.29	0.75	1.48	2.73	2.36	2.43	2.66	1.18	1.79	1.01	0.42	1.60	0.43	0.30	0.73	0.79	0.77		1.29
Tb	<0.03	<0.03	<0.03	0.14	0.30	0.47	0.55	0.40	0.52	0.24	0.29	0.19	0.05	0.23	0.06	0.03	0.04	0.16	0.12	0.11	0.15
Dy	<0.05	<0.05	<0.05	0.84	1.53	2.36	3.25	3.38	4.27	1.66	2.16	1.22	0.39	1.62	0.35	0.04	0.11	1.51	1.18	0.68	0.97
Ho	<0.03	<0.03	0.03	0.21	0.32	0.47	0.73	0.93	1.15	0.51	0.54	0.40	0.19	0.37	0.10	0.08	0.08	0.43	0.46	0.28	0.22
Er	<0.05	<0.05	0.05	0.55	0.81	1.24	1.93	2.52	3.01	1.34	1.46	1.03	0.49	0.86	0.26	0.23	0.15	1.35	1.29	0.70	0.70
Tm	<0.03	<0.03	<0.03	0.11	0.15	0.25	0.35	0.41	0.46	0.20	0.20	0.17	0.05	0.12	0.03	0.03	<0.03	0.18	0.18	0.10	0.09
Yb	<0.01	<0.01	0.12	0.83	0.95	1.76	2.66	2.84	2.47	1.20	1.32	0.99	0.32	0.81	0.18	0.22	0.11	0.99	0.95	0.48	0.70
Lu	<0.01	<0.01	0.01	0.14	0.17	0.26	0.43	0.40	0.37	0.17	0.23	0.16	0.06	0.10	0.03	0.03	0.02	0.15	0.14	0.08	0.12

See Table 5 for a description of the samples. LOI: loss on ignition. Methods of analysis: major elements by X-ray fluorescence (XRF), CO₂ by coulometric titration, minor elements by inductively coupled plasma – mass spectrometry (ICP–MS) except those elements indicated by an asterisk, by XRF. † All results were obtained by ICP–MS analysis. †† Sum with Mn expressed as Mn_2O_3, Ba as $BaSO_4$, and Sb as Sb_2O_5. Low analytical totals are observed for some samples containing elements in concentrations much higher than the range of calibration, in particular JB131 (P) and JB423 (Sb). Some carbonates (JB175 and JB320) also tend to have low totals. Samples: JB174: near Fianel, Triassic marble. JB175: near Fianel, white marble. JB120: Samada Sura, aegirine skarn. JB160: Martegn, aegirine skarn. JB122: Samada Sura, Fe-carbonate ore (ankerite-rich). JB124: Samada Sura, Fe-carbonate ore, siderite-rich. JB156: Martegn, Fe-carbonate ore. JB131: Bergwiesen, apatite schist. JB133: Bergwiesen, Hem–Qtz ore. JB100: Fianel, Hem–Qtz ore. JB101: Fianel, Hem–Qtz–carbonate ore. JB105: Fianel, Hem–Qtz ore. JB147: Fianel, medaite-bearing mixed ore. JB302: Fianel, pyroxenite. JB320(†): Fianel, pink carbonate clast (Be–Mo–W breccia). JB306: Starlera, Hem–Qtz–carbonate ore. JB92: Piz La Mazza, Hem–Qtz–carbonate ore. JB337.1: Schmorrasgrat, oxide ore. JB407: Schmorrasgrat, oxide ore. JB423: Val Sterla, roméite-bearing ore. Compositions expressed in weight % (major elements) and ppm (trace elements).

TABLE 5. DESCRIPTION OF THE SAMPLES IN THE VAL FERRERA SUITE
FOR WHICH CHEMICAL COMPOSITION IS LISTED IN TABLE 4

Sample	Deposit	Rock type	Mineralogy
Triassic marble			
JB174	near Fianel	Pink marble (stained by Hem)	Cal, Dol ± Tlc, Ms, Hem
JB175	near Fianel	White marble	Cal ± Qtz, Ms
Fe-carbonate veins in augen gneiss			
JB120	Samada Sura	Ae–Mgt skarn	Qtz, Mgt, Ae, Ms ± amphibole (winchite)
JB160	Martegn	Ae–Hem skarn	Qtz, Hem, ± Ae, Ms
JB122	Samada Sura	Ank-rich Fe-carbonate ore	Qtz, Ank, Ms
JB124	Samada Sura	Sd-rich Fe-carbonate ore	Sd, Ank, ± Qtz, Ms
JB156	Martegn	Fine grained Fe-carbonated ore	Qtz, Ms, Ank, Sd
Carbonate-hosted deposits			
JB131	Bergwiesen	Apatite schist	Ap, Kth, Qtz, Ms, ± Tlc, Cal
JB133	Bergwiesen	Finely laminated Hem–Qtz ore	Qtz, Hem, ± Ms
JB100	Fianel	Hem–Qtz ore	Qtz, Hem, ± Ms
JB101	Fianel	Hem–Qtz–carbonate ore with pink carbonate clasts	Qtz, Hem, Dol, Tlc, ± Ms
JB105	Fianel	Hem–Qtz ore	Qtz, Hem, ± Ms, Tlc
JB147	Fianel	Med-rich mixed ore	Qtz, Hem, ± Med, Ms, Ae, Kth, Rds, Brt
JB166	Fianel	Mixed ore	Qtz, Hem, ± Rdn, Ae, Ms, Tlc, Ap
JB302	Fianel	Pyroxenite	Ae, Qtz, Dol, Cal, Brt, Ap
JB320	Fianel	Pink Dol clast from the Be–Mo–W breccia	
JB306	Starlera	Hem–Qtz–carbonate ore	Hem, Qtz, Brn, pyrolusite(?), Cal
JB92	Piz La Mazza	Schistose Hem–Qtz–carbonate ore	Qtz, Hem, Kth ± Ms, Tlc
JB337.1	Schmorrasgrat	Johninnesite-bearing oxide ore	Hem, jacobsite, Kth ± amphibole (winchite), Dol, Kth
JB407	Schmorrasgrat	Jacobsite ore	jacobsite, Hem, amphibole, Ms
JB423	Val Sterla	Roméite-bearing ore	Ank, Ap, Qtz, ± Hem, Cal, Ms, Brt

The minerals listed are those identified by X-ray powder diffraction.

hydrothermal fluids to mobilize Fe from the augen gneiss. Thus, the augen gneiss is also a likely source for the Fe in the pre-D_1 Fe-carbonate veins. Differences between the *REE* patterns of Fe-carbonate veins and augen gneiss (Fig. 12a) can be explained by derivation of both the Fe and *REE* in the veins from the augen gneiss. *REE* are transported as complexes in hydrothermal fluids. The stability of the strong complexes with OH^- and F^-, and therefore the solubility of the *REE*, increase as the ionic radius of the *REE* decreases (Haas *et al.* 1995). However, weaker chloride, carbonate, or hydrocarbonate complexes are more likely to have been present in the fluids involved in the formation of the Fe-carbonate veins. The stability of these complexes changes only slightly with ionic radius of the *REE*, and thus would not explain the observed changes in La:Lu ratio between veins and augen gneiss. In addition to complexing, crystallographic control may also have been an important, perhaps even a dominant, factor in controlling the *REE* pattern of the Fe-carbonate ores. Siderite is likely to favor incorporation of the *HREE* owing to the small ionic radius of Fe^{2+} ($^{VI}r = 0.78$ Å;

Shannon 1976) relative to the radii of the other *REE*. The positive Eu anomaly in the veins is explained by the preferential alteration of plagioclase in the augen gneiss, as this mineral commonly displays a positive Eu anomaly (*e.g.,* Lipin & McKay 1989).

Aegirine skarns developed locally during metamorphism at the contact between Fe-carbonate veins and augen gneiss host-rock. Where these skarns have a low Na content, they have a *REE* pattern parallel to that of the siderite ore (Fig. 12a). In this case, the skarn seems to have replaced carbonate ores, and the *REE* were essentially immobile. At higher levels of Na, however, the skarns display a strong *HREE* depletion (Fig. 12a). Normal Fe-carbonate ores have low Na contents (<0.05 wt% Na_2O), and therefore, the Na in the skarn had to be carried by the fluid responsible for skarn formation. The correlation between high Na content and *HREE* depletion in the aegirine skarns indicates that the metasomatic fluid responsible for Na enrichment has also preferentially removed *HREE* from the Fe-carbonate ore. Fluid flow in D_1 shear zones within the Roffna porphyry induced breakdown of albite, releasing Na into the fluid.
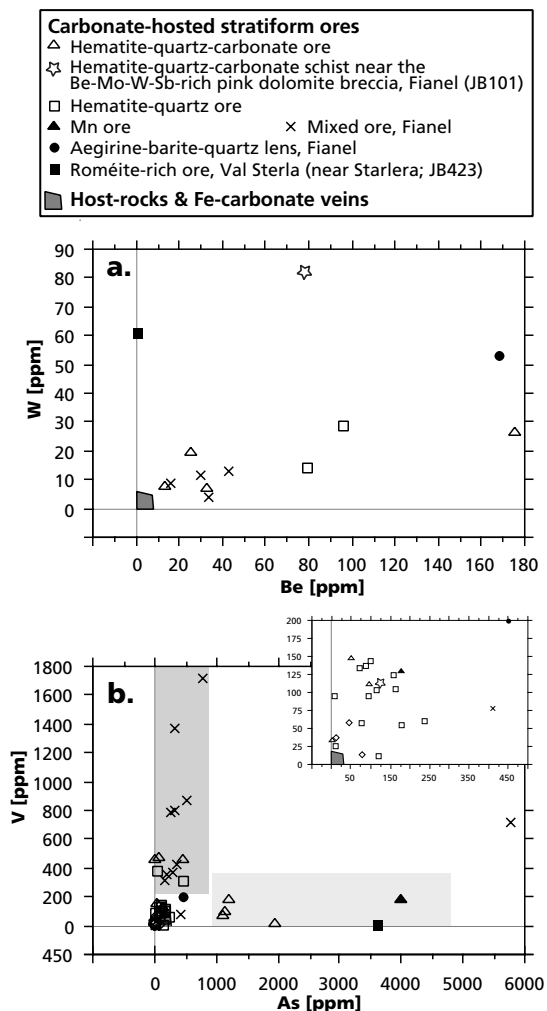
FIG. 10. Variation diagrams for the whole-rock composition of the Fe–Mn ores of Val Ferrera. (a) W *versus* Be; (b) V *versus* As. The shaded areas labeled "host-rocks & Fe-carbonate veins" in each diagram mark the compositional range of Triassic marbles (five analyses) and ores from the Fe-carbonate veins in the Suretta nappe basement (five analyses). The hematite – quartz – carbonate ores and the hematite–quartz ores were collected from all deposits in Val Ferrera, including the four localities discussed in this paper (Table 5). The two samples of Mn ore are from the Schmorrasgrat locality (Brugger & Berlepsch 1997). Data from Table 4 and from Brugger (1996).

Furthermore, overgrowths of Y- and *HREE*-rich minerals around grains of zircon in the shear zones document the ability of this fluid to mobilize *HREE* (Vocke *et al.* 1987). A similar metamorphic fluid probably interacted with the Fe-carbonate veins to form the skarn.

Age of the carbonate-hosted stratiform Fe–Mn mineralization

Occurrence of hematite–quartz pebbles in synsedimentary Mesozoic (Liassic–Cretaceous?) breccias implies synsedimentary to diagenetic formation of the stratiform ores hosted by the Triassic carbonates. The concordant nature of the orebodies and their internal structures, particularly the finely laminated alternations of ore and carbonate, suggest a syngenetic origin of the mineralization. This conclusion, which is based on field relations, is supported by some of the microtextural observations presented here. The carbonate–muscovite spherules at Piz La Mazza might represent relict sedimentary structures, *e.g.*, pellets or clay aggregates; the latter may have been important in scavenging certain elements. In particular, sorption on clays could explain the enrichment of the spherules in Y and P [*e.g.*, Aja (1998) for *REE*]. At Bergwiesen, the tiny crystals of arsenian fluorapatite preserved within spessartine porphyroblasts are consistent with the fine-grained nature of syngenetic ores (*e.g.*, Binns *et al.* 1993, Hein *et al.* 1994).

The growth of minerals such as långbanite, medaite, arsenian fluorapatite, and barylite in the main S_1 schistosity of the Fianel ores indicates that the elements Sb, V, As, Be, and Ba were present in the rocks during D_1. No syn-D_1 mineral of tungsten was observed, but the trend linking W and Be (Fig. 10a) suggests a genetic link between these elements. Vanadium and As are characteristic of many syngenetic Mn deposits, and the presence of high As contents has been considered diagnostic of the exhalative origin of syngenetic deposits (Marchig *et al.* 1982). A positive correlation between the levels of As and Sb has been observed in some recent metalliferous sediments of volcanogenic hydrothermal origin (*e.g.*, Karpov & Naboko 1990, Pearcy & Petersen 1990). In our samples, the correlation is poor, but in general, the As contents are higher where the Sb contents are elevated. Mobility of Be and W in epithermal systems is documented by the large deposits of bertrandite in Utah (Staatz & Carr 1964), and by some active continental hydrothermal systems such as Waiotapu, New Zealand (Hedenquist 1983) and Uncia, Bolivia (White 1974). Thus it seems likely that the carbonate-hosted stratiform Fe–Mn deposits in Val Ferrera became enriched in Sb, As, V, Be, and W during ore formation. Alternatively, some or all of these elements may have been transported into the orebodies at a later stage, *e.g.,* by epithermal or metamorphic fluids that reacted with the Fe–Mn ores. However, there is no evidence to support such a two-stage history. In the study area, no post-Triassic magmatic activity is documented that could have produced such fluids. In particular, the intrusion of the Bergell granodiorite clearly postdates D_2 and thus also enrichment of the ores in Sb, As, V, Be, Ba, Sr, and W. Moreover, all of the investigated carbonate-hosted deposits display similar geochemical features, such that
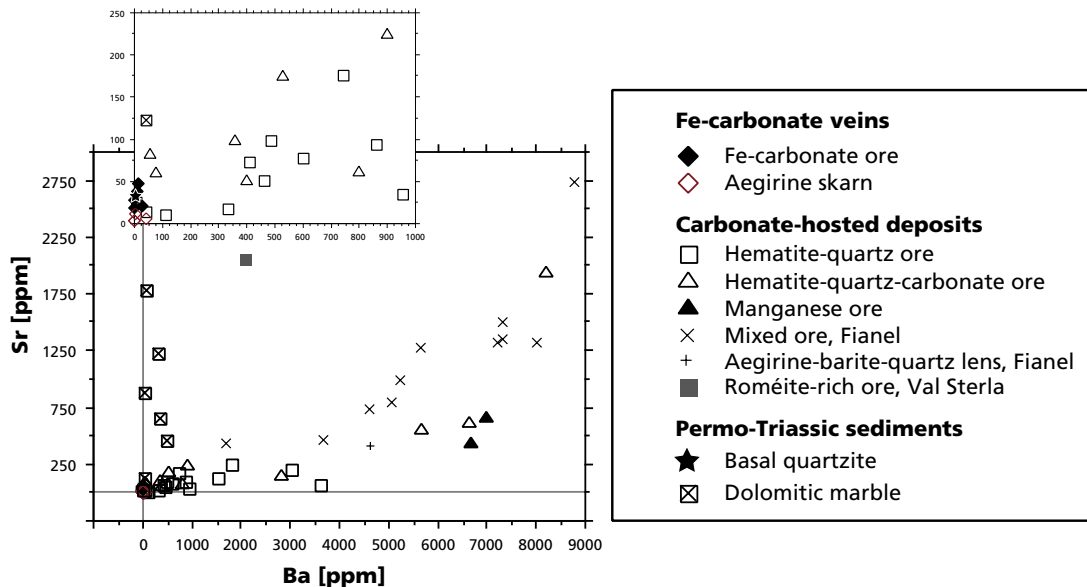
FIG. 11. Sr *versus* Ba variation diagram showing the compositional trends of the various types of ore. Data from Table 4 and from Brugger (1996).

any postulated post-ore event must have acted on a regional scale. In Val Ferrera, however, mineralization indicative of the presence of such fluids occurs exclusively in the carbonate-hosted stratiform Fe–Mn ores. In particular, no evidence is found in rocks such as the pre-D_1 Fe-carbonate veins (Figs. 10a, b) or the calc-schists of the Suretta and Starlera nappes (Fig. 2), which likely would have reacted with such a regional fluid. On this basis, we conclude that enrichment of the ores in these trace elements occurred simultaneously with ore formation.

Transport and deposition of metals into the carbonate-hosted stratiform deposits

The wide range of Fe/(Fe + Mn) values found in the carbonate-hosted deposits contrasts with the restricted range observed for the Fe-carbonate veins (Fig. 9). Krauskopf (1957) showed that a separation between Fe and Mn can arise from the different relative stabilities of Fe and Mn oxyhydroxy-minerals as a function of Eh and pH. For example, a progressive oxidation of a reducing fluid generates first the precipitation of Fe, and later the precipitation of Mn. The strong redox gradient located near the sediment–seawater interface is a favorable location for such a process, as is demonstrated by modern-day black smokers (Bonatti 1975).

Metals in syngenetic Fe–Mn deposits can be derived either from seawater (hydrogenetic) or from sub-sea-

floor sources (exhalative). In the latter case, Huebner *et al.* (1992) distinguished between hot hydrothermal fluids and cold diagenetic fluids. Many variation diagrams have been developed to discriminate between a hydrogenetic and an exhalative origin of the metals in syngenetic Fe–Mn ores. In our opinion, however, most of these diagrams are of little value for carbonate-hosted deposits. In particular, the classic triangular Mn–Fe–(Co + Ni + Cu) diagram of Bonatti *et al.* (1972) was developed for deep-sea deposits, where rates of sedimentation are low. The Val Ferrera ores plot in the hydrothermal field of this diagram (low content of transition metals), but so do Swiss oolitic and residual ores (Serneels 1993, and unpublished data by Serneels), which are unlikely to have a significant (if any) hydrothermal component. Similarly, the Val Ferrera ores plot in a restricted area within the hydrothermal fields in the diagrams Si *versus* Al (Crerar *et al.* 1982), Fe:Ti *versus* Al, and Mn:Ti *versus* Al (Barrett 1981). These latter diagrams, again, were developed for deep-sea environments, and reflect the competition between rapid deposition of Si, Fe, and Mn from hydrothermal fluids and slow input (below the calcite-compensation depth) of detrital Ti and Al. These diagrams, therefore, are not suitable for deposits forming on a carbonate platform, where sedimentation is much faster and dominated by biogenic carbonates.

On the other hand, the presence of significant quantities of As, Sb, W, and Be strongly suggests a hydro-
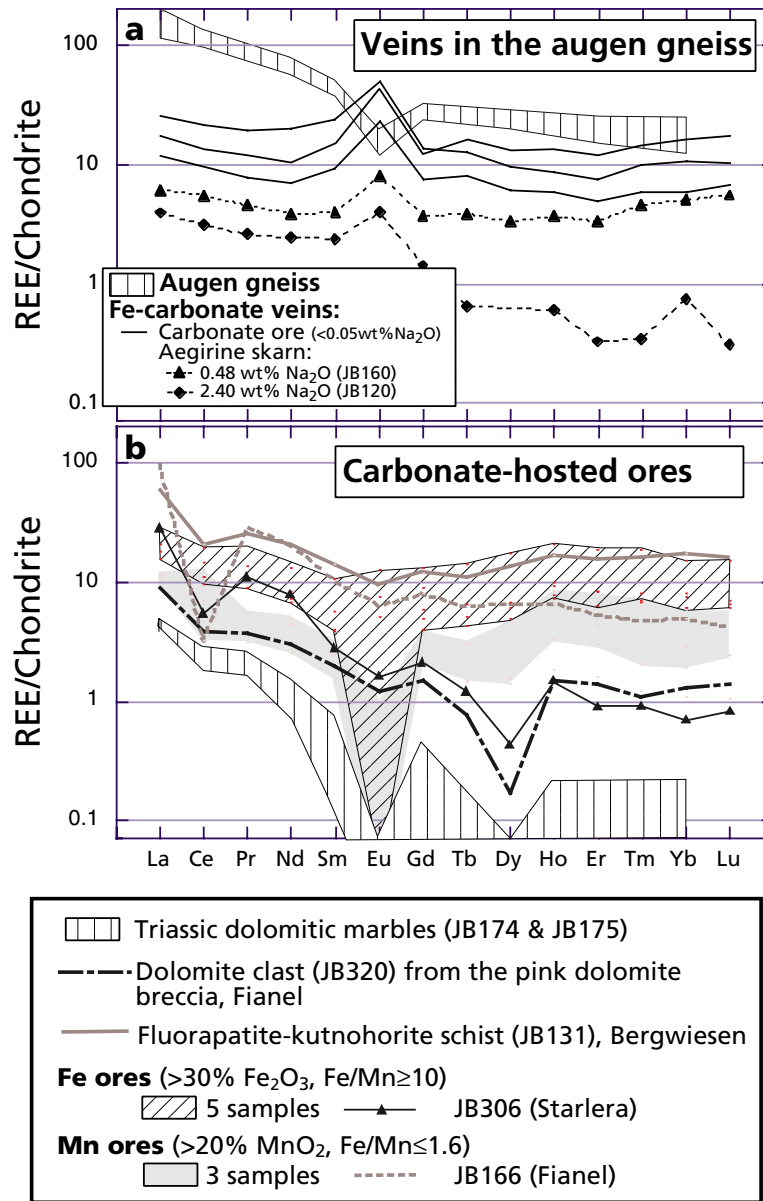
FIG. 12. Chondrite-normalized *REE* patterns of (a) ores from the siderite veins, compared to the augen gneiss analyses of Vocke *et al.* (1987), and (b) Mn and Fe ores from Val Ferrera, compared to those of the carbonate host-rocks. Chondrite data from Evensen *et al.* (1978).

thermal component in the carbonate-hosted deposits. The Sr *versus* Ba diagram (Fig. 11) suggests different sources for Sr and Ba. The Sr contents of the ores are similar to those of the enclosing carbonates; Ba contents, however, are generally much higher in the ores. Barite

is the main carrier of Ba and Sr in the ores and, according to Putnis *et al.* (1992), its Ba/Sr depends on the Ba/Sr value in the fluid. The positive correlation between Sr and Ba in the ores (Fig. 11) could thus be explained by precipitation of barite, a process that most likely takes

place where Ba-rich, sulfate-free hydrothermal waters mix with Sr- and sulfate-rich seawater.

The *REE* patterns of the carbonate-hosted ores plot between those of two end members, one defined by Fe ores ($La_{CN}/Lu_{CN} \approx 1$), and the other by the Triassic marble host-rocks ($La_{CN}/Lu_{CN} \gg 1$); data for the Mn ores typically plot in between (Fig. 12b). At first glance, this position seems to indicate mixing between a hydrothermal fluid and seawater (*cf*. Fig. 13a for modern analogue), and such simple relationships have been invoked, for example, to explain systematic variations in the *REE* patterns of banded-iron formations (Kato *et al.* 1998). One anomalous, Fe-rich sample (JB306), however, plots close to the enclosing marbles, and its *REE* pattern is very similar to that of a dolomite clast from the pink dolomite breccia at Fianel (Fig. 12b). Some modern hydrothermal sediments have *REE* patterns and contents that are similar to those of the carbonate-hosted ores from Val Ferrera (Fig. 13b). In particular, the Fe ores from Val Ferrera exhibit a strong similarity to nontronite-rich Fe oxyhydroxide sediments in seafloor chimneys and mounds, which are characterized by concave *REE* patterns, slightly negative or no Ce anomalies, and negative Eu anomalies (Hekinian *et al.* 1993; Fig. 13b). The anomalous Fe-rich sample (JB306) has a *REE* pattern similar to those reported for Fe-sulfide mud and silica-rich Fe oxyhydroxides from the East Pacific rise (Fig. 13b). These modern samples probably do not contain a significant hydrogenetic component (Hekinian *et al.* 1993), reflecting the importance of mineralogical controls on the *REE* patterns of the sediment. Therefore, it appears difficult to interpret quantitatively the *REE* patterns of metamorphosed deposits, where the original mineralogy of the sample and its location relative to submarine vents are obscured. This problem is exacerbated, in our case, by the fact that the depositional environment of the Val Ferrera ore (shallow carbonate platform) was very different from that of the deep oceanic deposits. Nevertheless, similarity of the *REE* patterns of the Val Ferrera ores with those of modern proximal hydrothermal sediments strongly suggests that they share a similar exhalative origin.

Variability of the Eu and Ce anomalies furnishes a strong argument for ore formation at a pronounced redox boundary, such as that existing at the interface between sediment and seawater. The strongly oxidizing conditions required for the stability of Ce^{4+} are rarely obtained in the Earth's crust. Oxidation of Ce^{3+} to Ce^{4+} does occur in seawater, even if the precise mechanisms involved remain unclear. Equilibrium thermodynamics (Liu *et al.* 1988), surface reactions on Mn oxyhydroxides (Brookins 1989 and references therein), and bacterial activity (Moffett 1990) all have been invoked. Repeated precipitation (at the contact with seawater) and redissolution (as burial brings the newly formed chemical sediment to reducing conditions) may produce the random Eu and Ce anomalies observed in the carbonate-hosted ores.

No trace of volcanic or magmatic activity could be observed in the marbles in proximity to the studied deposits. Concordant layers of amphibolite, however, occur in the dolomitic marbles of the southern part of the Suretta nappe and probably represent meta-tuffs (Gieré 1985). Similarly, the thick Triassic series (about
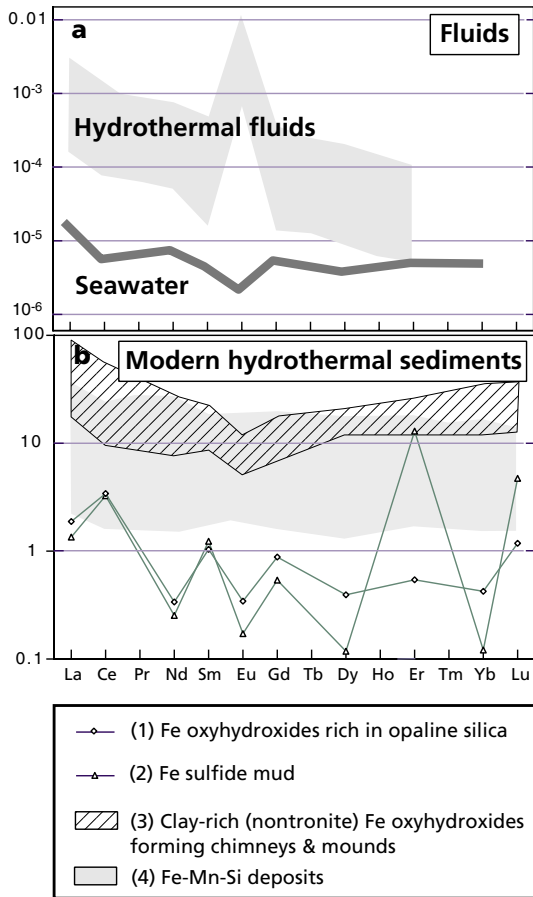

FIG. 13. Chondrite-normalized *REE* patterns of fluids, seawater and modern sediments. (a) Patterns for seawater (Atlantic, 2500 m: Elderfield & Greaves 1982) and hydrothermal fluids from the Mid-Atlantic Ridge at 37%17'N (Klinkhammer *et al.* 1995). (b) Recent and modern Fe and Mn sediments from mid-oceanic ridges and oceanic intraplate volcanoes. (1) Sample ALV–1996–6–2, East Pacific Rise axis at 11°30' N (Hekinian *et al.* 1993). (2) Sample CY82–14–4, East Pacific Rise axis at 12°50'–12°43' N (Hekinian *et al.* 1993). (3) Samples TH3–6 [South Pacific intraplate volcano], CY82–7–13 [East Pacific Rise at 12°50'–12°43' N], and NZ18–12 [Galapagos Triple Junction] (Hekinian *et al.* 1993) (4) Franklin seamount, western Woodlark Basin, Papua New Guinea (Binns *et al.* 1993). Chondrite data from Evensen *et al.* (1978).

600 m) of the Tschera–Kalkberg 2b unit (Rück 1995) in the Schams Nappes contains many tuffaceous layers; these are particularly abundant in the Upper Anisian (where a pumice layer is present) and Lower Ladinian, but occur also in the Lower and Middle Anisian as well as in the youngest Upper Ladinian (Streiff *et al.* 1976). Moreover, synsedimentary tectonic movements are documented in the Triassic of the Schams nappes, for example, by different transgressive horizons and by the occurrence of monogenic and polygenic breccias (Streiff *et al.* 1976). Therefore, we conclude that the thermal conditions and tectonic setting for the activation of distal epithermal systems within the Suretta basement were present during the Triassic.

On the basis of the arguments presented above, the carbonate-hosted deposits most likely represent Triassic synsedimentary exhalative deposits, and the As, Sb, V, Be, W, Ba, Sr, and the *REE* were introduced simultaneously with the Fe and Mn oxyhydroxide minerals. Most elements were supplied by a hydrothermal fluid that circulated in the basement. Exceptions are S and possibly Sr, which are considered to be derived mainly from seawater.

Premetamorphic mineralogy of the carbonate-hosted ores

By analogy with modern seafloor syngenetic exhalative deposits, such as on Franklin Seamount in the Western Woodlark Basin (Binns *et al.* 1993), the original mineral assemblage of the Val Ferrera deposits may have comprised carbonates, Fe–Mn hydroxides and oxides, silica, and strontian barite. The elevated Na content of some Fe–Mn ores in Val Ferrera could be related to primary minerals such as vernadite [δ-(Mn,Fe,Ca,Na)(O,OH)$_2$•nH$_2$O], birnessite [Na$_4$Mn$_{14}$O$_{27}$•9H$_2$O], and nontronite [Na$_{0.3}$(Fe^{3+})$_2$(Si,Al)$_4$O$_{10}$(OH)$_2$•nH$_2$O], which are major constituents of some Fe–Mn crusts of hydrogenetic and hydrothermal origin (Bolton *et al.* 1988, Binns *et al.* 1993). Sodium enrichment also is known from other places in the Suretta cover: farther south, for example, at Roticcio in Val Bregaglia, sodic amphiboles occur in close association with Fe oxides within the Triassic carbonates (Gieré 1985). It is not possible, however, to exclude a metasomatic input of Na during metamorphism. Na mobility during D$_1$ is described by Vocke *et al.* (1987) in the granitic rocks, and by Oberhänsli (1978) in metabasalts from the Bündnerschiefer.

The high phosphorus contents of some Val Ferrera ores (up to 10.6 wt% P$_2$O$_5$ at Bergwiesen) also may be compared to those reported from the active hydrothermal vent deposits at Franklin Seamount (up to 5.3 wt% P$_2$O$_5$, Scott & Binns 1991). No discrete P mineral, however, was observed (by X-ray diffraction) in association with the Fe, Mn, and Si minerals from Franklin Sea-

mount, indicating that P is present either in amorphous phosphate phases, or as a minor component in some oxyhydroxides (Boyd & Scott 1999). Apatite thus probably forms only during diagenesis. Volcanogenic submarine Fe-rich sediments in the Tyrrhenian Sea (Gamberi *et al.* 1997) also contain up to 1.83 wt% P$_2$O$_5$. The elevated P contents of the Fe–Mn ores could be of hydrothermal or biogenic origin. In the Triassic marbles of the Suretta and Starlera nappes, no phosphorites are known, and the levels of P in the Fe–Mn ores may be the result of an uncommon biogenic activity near the hydrothermal vent, or of inorganic processes such as coprecipitation or sorption.

The major part of the Al, Ti, and Zr contained in the ores is probably related to detrital input of mica and clays, rutile and zircon, consistent with the rounded shape of the rutile and zircon grains. The TiO$_2$ (≤ 0.1 wt%) and Al$_2$O$_3$ (≤ 3.5 wt%) contents of the ores correspond to the range of values found in the marbles (Table 4), and are consistent with a maximum proportion of about 20 wt% crustal material (Taylor & McLennan 1985).

In syngenetic ores, elements like As (*e.g.,* Schaufelberger 1994, Manceau 1995, Manning & Goldberg 1997), V (Schwertmann & Pfab 1994) and, by analogy, Sb, may be fixed by sorption onto Fe and Mn oxides and hydroxides, as well as on mica and clay minerals. The affinity of As for Fe oxyhydroxides is particularly well established, and is also indicated by the coprecipitation of As with Fe oxides and hydroxides in acid mine-drainage waters (*e.g.*, Dzombak & Morel 1990). Elements with a large ionic radius (*e.g.*, Ba^{2+}) may be retained in minerals with tunnel structures, like todorokite [(Mn,Ca,Mg)Mn$_3$O$_7$•H$_2$O] and birnessite. At Bergwiesen, fluorapatite or its precursor phase may have been an important sink for As, whereas at Starlera, concordant segregations of tilasite in As-rich portions of the ore may be related to a syngenetic or diagenetic As-rich precursor phase. Such phases have not yet been reported from modern deposits, but abundant tilasite occurs in other metamorphosed Mn deposits. Dolomite–tilasite marble occurs in polymetamorphic Precambrian rocks at Nežilovo, Macedonia (T < 500°C, P > 2 kbar; V. Bermanec, written commun.); it is associated with a regional enrichment in Ba, Zn, Pb, Cu, Mn, Ti, *REE* and As attributed to syngenetic exhalative processes (Bermanec *et al.* 1993, Bermanec 1994). Tilasite-rich veins have also been described from the sediment-hosted, zeolite-facies-metamorphosed Mn ores at Djebel Guettara, Algeria (Heflik 1989). Tilasite thus occurs under very broad P–T conditions, and might even be a syngenetic to diagenetic phase in some deposits. Colloidal Mn oxyhydroxides from recent hydrothermal deposits contain up to 0.18 wt% W (Kirchheimer 1959), and Be can be hosted in rhodochrosite in considerable quantities (up to 0.3 wt% BeO, Grigor'yev 1967).

Genetic link between Fe-carbonate veins and sediment-hosted stratiform deposits?

The available lines of evidence do not allow us to reject a direct genetic link between the Fe-carbonate veins in the basement and the carbonate-hosted deposits; the former possibly acted as feeder channels for the latter. Both formed prior to the D_1 event, but no further clue to their relative age is available. The augen gneiss is a likely source for the Mn and Fe (and possibly other elements) found in both types of deposits. The pronounced difference in trace-element profile of these deposits can be explained in terms of the markedly different conditions of ore formation: (1) The Fe-carbonate veins were deposited within pre-Triassic orthogneisses of the basement; they acquired a simple assemblage (Fe-carbonate), where the minerals were probably well crystallized and relatively coarse-grained. In contrast, the carbonate-hosted deposits formed at or close to the sediment–seawater interface, comprising a complex association of poorly crystalline Fe–Mn oxyhydroxides. Adsorption most likely did not play a significant role during formation of the Fe-carbonate veins (higher temperature, unfavorable mineralogy, low surface-area), but it was a fundamental process during formation of the carbonate-hosted deposits, where elements like As, Sb, V, and possibly Be, W, and *REE* were scavenged. (2) In contrast to the Fe-carbonate veins, deposition of the carbonate-hosted ores took place in an environment with a pronounced redox gradient. This redox gradient was responsible for the separation of Fe and Mn, for variability of the Eu and Ce anomalies, and it may have controlled the deposition of other redox-sensitive trace elements (*e.g.*, As, V, Sb). (3) The presence of sulfate in seawater was most probably responsible for the precipitation of Ba and Sr as strontian barite; elements like Sr and S were likely partially derived from seawater.

Paragenetic evolution during metamorphism

Tertiary metamorphism induced recrystallization and breakdown of the primary Fe and Mn minerals. The behavior of Sb, As, V, and Be during D_1 was controlled by the mineralogical and geochemical composition of the protolith. In Fe-rich deposits, hematite can accommodate relatively high contents of As and V (*e.g.*, Piz La Mazza; Fig. 14). Indeed, a complete solid-solution exists between Fe_2O_3 and V_2O_3 (Cox *et al.* 1962). Thus, As and V were still highly compatible with regard to the metamorphic mineral (hematite), compared to the syngenetic phase (poorly crystalline Fe oxyhydroxide), inhibiting the formation of metamorphic arsenates and vanadates. Fluorapatite and its precursor phase played a similar role for As in the fluorapatite – kutnohorite – hematite schists of Bergwiesen (Fig. 15a). Arsenic is strongly compatible in fluorapatite, and metamorphic recrystallization did not release much arsenic. In contrast, Sb, As, V, and Be tend to accumulate in synkinematic accessory minerals in mixed ores at Fianel (Fig. 15b). Here, medaite, långbanite, barylite, and arsenian fluorapatite grew during D_1 metamorphism.

At Starlera, the only syn-D_1 As-bearing minerals found are fluorapatite with low As contents in the pink schists (Fig. 15d), and tilasite in some hematite – carbonate – quartz ores (Fig. 15e). No unambiguous syn-D_1 phase rich in Sb has been identified so far at Starlera; this contrasts with the large amounts of Sb contained in the discordant tilasite–roméite veins characteristic of this locality (Brugger *et al.* 1997). The pink schists at Starlera contain a complex mineral assemblage that evolved mainly after D_1, characterized by Sb, As, Be and *REE* minerals (Fig. 15d). Moreover, the Ti minerals titanite, pyrophanite, and some rutile grew after D_1 and incorporated considerable amounts of Sb and As, thus recording elevated contents of these metals in a post-D_1 fluid. Post-D_1 remobilization of certain elements (*i.e.*, V, As, Be) is further documented by the mineralogy of discordant veinlets and open fractures in the mixed ores at Fianel (Fig. 15b). Also at Fianel, a lens of dolomitic breccia contains Sb, As, Be, Mo, and W minerals in discordant veinlets and in pressure shadows of dolomitic clasts (Fig. 15c); a metasomatic event subsequently led to the formation of paraniite-(Y) within the scheelite–powellite, and of As-rich fluorapatite along the rim of fluorapatite grains (Fig. 15c; *cf.* Brugger *et al.* 1998). The latest stage of the metamorphic evolution produced narrow open fractures in the Fianel deposit: in the mixed ores, the fractures contain fianelite (Brugger & Berlepsch 1996), which formed as a product of weathering of nearby palenzonaite (Fig. 15b), whereas in the dolomite breccia the open fractures host powellite crusts, scheelite–powellite, chernovite-(Y), and barite (Fig. 15c; Brugger *et al.* 1998).

The post-D_1 history of the mobilization of the trace elements is indeed complex. A major problem results from the difficulty of correlating the paragenetic successions found in different types of ore with each other, and with the regional tectonometamorphic evolution. The complex mineralogy of the Fe–Mn ores contrasts strongly with that of the country rocks; the latter consist of granitic gneisses and marbles that were mineralogically relatively inert following D_1. The complex discordant veins that are common in the Mn ores have no equivalent in the host rocks. The abundance of post-D_1 magnesioriebeckite in the breccia at Starlera also is a unique feature, which might be related to hydrothermal fracturing during D_2 deformation; thick roméite–tilasite veins of the Starlera deposit could also be attributed to this event (Fig. 15e). The unusual mineralogy of the pink schists is due to their characteristically high Ti content, which is probably mainly the result of a high proportion of detrital components in the protolith (*cf.* rounded grains of rutile). This high primary Ti content also renders the pink schists a likely source for the Ti in roméite of the late roméite–tilasite veins. In addition, the pink schists represent preferential flowpaths for fluids that
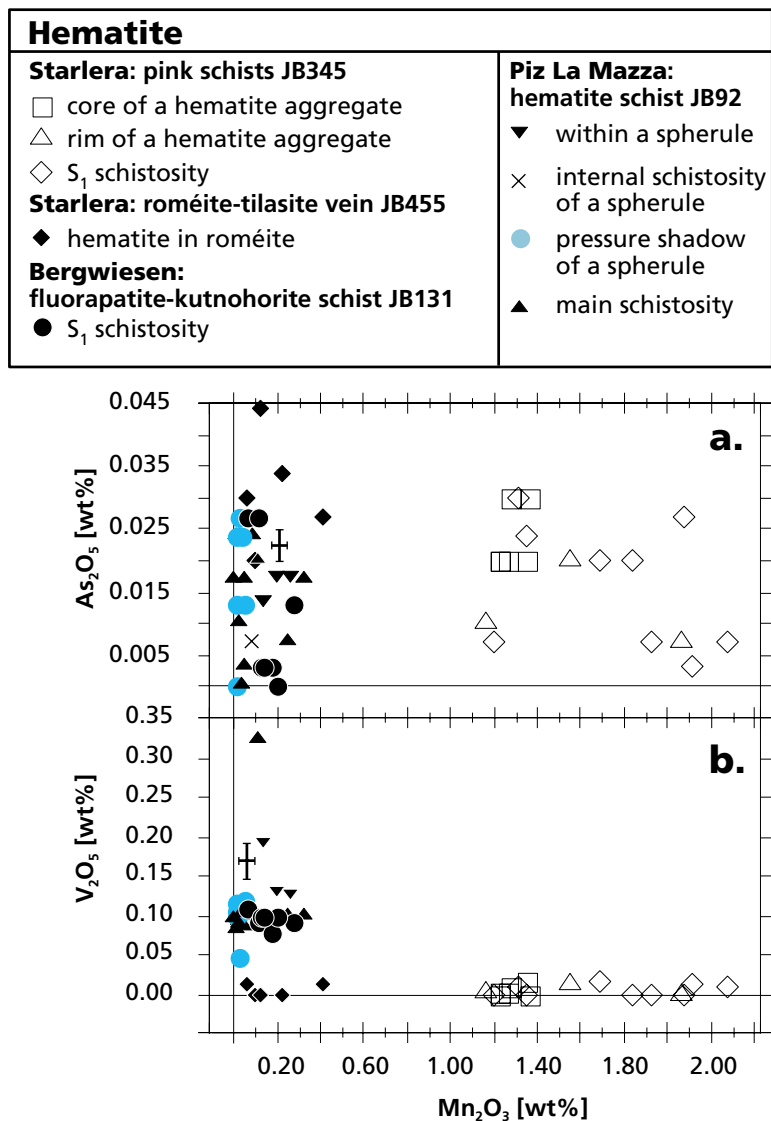
Hematite	
Starlera: pink schists JB345	**Piz La Mazza:** **hematite schist JB92**
□ core of a hematite aggregate	▼ within a spherule
△ rim of a hematite aggregate	× internal schistosity of a spherule
◇ S$_1$ schistosity	🔵 pressure shadow of a spherule
Starlera: roméite-tilasite vein JB455	▲ main schistosity
◆ hematite in roméite	
Bergwiesen: **fluorapatite-kutnohorite schist JB131**	
● S$_1$ schistosity	

FIG. 14.   As$_2$O$_5$, V$_2$O$_5$ and MnO contents of hematite (electron-microprobe data; data from Brugger (1996). Error bars correspond to 2σ errors resulting from counting statistics.

eventually produced the roméite–tilasite veins, and the post-D$_1$ growth of Sb-rich titanite and stiboan rutile; growth of associated minerals in the matrix of the pink schists (Fig. 15d, "post-kinematic") may be related to this fluid.

Comparison with other metamorphosed
Fe–Mn deposits

The carbonate-hosted stratiform Fe–Mn deposits of Val Ferrera share many mineralogical and geochemical features with the Carboniferous Mn deposits in the central Pyrénées. Detailed textural and structural investigations led Ragu (1990) to infer a syngenetic exhalative origin for these deposits, which were subsequently subjected to a Hercynian upper-greenschist-facies regional metamorphism. Intrusion of large volumes of late Hercynian granites produced a second metamorphism under greenschist-facies conditions. The deposits of the Pyrénées are characterized by high V and Ba concentrations (no whole-rock data exist for Sb, As, Be, and W), and in some of these deposits As, V, Be, and W

	Trias - Lias	Syn-D1	Syn-D2 ?	Pre to syn-D4 (correlation between deposits speculative)	
a. Bergwiesen Fluorapatite - kutnohorite schist	**Syn-genetic/ diagenetic** fluorapatite (arsenian?) carbonate silica hematite detrital mica/clay	**Main schistosity S₁** arsenian fluorapatite kutnohorite quartz hematite spessartine		**Discordant veins** quartz beryl chalcopyrite	
b. Fianel Mixed ores	**Syn-genetic/ diagenetic** carbonates Fe-oxides and hydroxides Mn-(Na)-oxides and hydroxides silica strontian barite fluorapatite (As?)	**Main schistosity S₁** rhodochrosite, kutnohorite aegirine, spessartine, calderite, tephroite, rhodonite hematite, braunite, jacobsite quartz strontian barite barylite medaite V-Ba-Sr-phase arsenian fluorapatite långbanite		**Discordant veins** rhodochrosite, kutnohorite aegirine, spessartine, calderite, rhodonite, parsettensite, Na-amphibole hematite quartz strontian barite beryl palenzonaite saneroite pyrobelonite medaite	**Open fractures** aegirine quartz barite fianelite
c. Fianel Pink dolomite breccia			**Discordant veins** quartz, dolomite scheelite-powellite beryl, bergslagite, betafite,fluorapatite, roméite strontian barite	**As-LREE metasomatism** paraniite-(Y) arsenian fluorapatite As-REE-rich roméite	**Open fractures** quartz, dolomite powellite, scheelite-powellite, chernovite-(Y) barite
d. Starlera Pink schists	**Syn-genetic/ diagenetic** **Exhalative origin** silica Fe oxide/hydroxide strontian barite fluorapatite (As?) **Detrital origin** clay minerals/mica zircon rutile	**Main schistosity S₁** quartz hematite strontian barite As-poor fluorapatite ? roméite Fe-Mn-white mica zircon rutile ?pyrophanite	**Post-kinematic** quartz As-rich fluorapatite roméite bergslagite stibian rutile pyrophanite stibian titanite aegirine		**Fractures in titanite** As-rich fluorapatite bergslagite stibian rutile pyrophanite
e. Other lithologies	**Concordant lenses** ? ? ? tilasite	**Thick veins** tilasite, roméite, aegirine, calcite, phlogopite, fluorite		

FIG. 15.   Synopsis of the paragenetic evolution in some Fe–Mn deposits and ore types from Val Ferrera. (a) Bergwiesen, fluorapatite – kutnohorite – hematite schist; (b) Fianel, "mixed ores"; (c) Fianel, pink dolomite breccia; (d) Starlera, pink schists; (e) Starlera, other lithologies. The correlations among the post-D₁ parageneses in the different deposits and rock types are not well constrained: the discordant veins in (a) and (b) are most likely synchronous, but the temporal relationship between these veins and the post-S₁ features shown in (c) and (d) are unknown. At Fianel, the open fractures in the mixed ores (b) are probably younger than those in the pink dolomite breccia (c). The horizontal shading emphasizes minerals that are stable over different stages (light gray), as well as the evolution of the carriers of trace elements like Be and V at Fianel (darker shade).

minerals occur in discordant veinlets (Ragu 1990, 1994, Brugger *et al.* 1999). Ragu (1994) argued that the elemental association found in these veins implies an input of at least Be and W from hydrothermal fluids originating in late Hercynian granites. The example of Val Ferrera suggests, however, that the Sb + As + V + Be + W association may also develop in a syngenetic environment. Thus, the occurrence of this association of elements in metamorphic veins should not be used as the sole geochemical indicator for a magmatic origin of the metamorphic fluids.

The mineralogy of the Val Ferrera ores is similar to that of radiolarite-hosted deposits in the Central Alps (*e.g.,* Falotta, Praborna) and in the Ligurian Alps. The mineralogical resemblance points to similarities in metamorphic evolution, but also in the geochemical composition of the protolith. Noteworthy is the fact that the two types of deposits formed under very different conditions, *i.e.*, near a mid-oceanic ridge over basaltic rocks (radiolarite-hosted deposits), and on a carbonate platform above a granitic basement (Val Ferrera deposits). Therefore, the hydrothermal fluids must have acquired their metal contents through interaction with markedly different types of rock. Similarity of the ore composition is probably a consequence of the similar conditions that existed during ore deposition (mixing of hydrothermal fluid with seawater) and of the processes responsible for enrichment of the trace elements considered (control by ore mineralogy). The particularly high Be and W contents of the Val Ferrera ores, on the other hand, can be related to occurrence of the deposits above a basement characterized by abundant rhyolites and granites. Remobilization of Be and W, together with As and *REE*, from Early Permian rhyolites has recently been documented also in other parts of the Alps (Knill 1996). Moreover, the Mn mineralization at Guettara, Algeria, is associated with Precambrian rhyolites and is particularly rich in As and Be (Agard 1965). Similarly, the Mn deposits at Långban (Boström *et al.* 1979) and Franklin (Dunn 1995) occur in carbonates deposited on continental crust and are well known for their Be and W minerals.

Comparison with element mobility in other geological settings

The joint mobility of high-field-strength elements (*HFSE*), large-ion lithophile elements (*LILE*), and *LREE* has been reported under very different P–T conditions and geodynamic settings, such as in subduction zones (*e.g.,* Sorensen & Grossman 1989, Philippot & Selverstone 1991) and within the mantle (*e.g.,* Harte 1987). These examples are of particular interest because there metasomatism affects the global geochemical cycles of various elements. In both cases, metasomatism is closely associated with magmatism. Volatiles reduce the solidus temperature, and, by altering the composition of the source region of magmas, metasomatism also influences the chemistry of the magmas (Lehmann *et al.* 1994).

A common feature of the element mobility in Val Ferrera, in subduction zones and in mantle metasomatism, is the importance of the stability of Ti minerals in controlling element mobility: titanite, rutile, and roméite in Val Ferrera; titanite and rutile in subduction zones (Philippot & Selverstone 1991), and titanian magnetite, titanite, crichtonite, armalcolite, and hollandite-type structures in mantle metasomatism (Harte 1987, Ionov *et al.* 1999). The structural properties of some of these minerals ensure that they are a major sink for both *HFSE* (in the Ti site), *LILE*, and *LREE* (in interstitial sites).

REFERENCES

AGARD, J. (1965): Découverte de béryllium dans la minéralisation du gîte de wolfram, molybdène et cuivre d'Azegour (Haut Atlas, Maroc) et dans celle du gîte de manganèse de Guettara (Sud algérien). *C.R. Acad. Sci. Paris* **261**, 4179-4180.

AJA, S.U. (1998): The sorption of the rare earth element, Nd, onto kaolinite at 25°C. *Clays Clay Minerals* **46**, 103-109.

BALZER, D. (1989): *Petrographie, Geochemie, Tektonik, Metamorphose und Geochronologie im nordwestlichen Teil der Suretta-Decke*. Diploma thesis, Univ. of Bern, Bern, Switzerland.

BARRETT, T.J. (1981): Chemistry and mineralogy of Jurassic bedded chert overlying ophiolites in the north Apennines, Italy. *Chem. Geol.* **34**, 289-317.

BAUDIN, T. & MARQUER, D. (1993): Métamorphisme et déformation dans la nappe de Tambo (Alpes Centrales suisses): évolution de la substitution phengitique au cours de la déformation alpine. *Schweiz. Mineral. Petrogr. Mitt.* **73**, 285-299.

————, ————, BARFETY, J.-C., KERCHKOVE, C. & PERSOZ, F. (1995): A new stratigraphical interpretation of the Mesozoic cover of the Tambo and Suretta nappes: evidence for early thin-skinned tectonics (Swiss Central Alps). *C.R. Acad. Sci. Paris* **321**, **IIa**, 401-408.

BERMANEC, V. (1994): Centro-symmetric tilasite from Nežilovo, Macedonia: a crystal structure refinement. *Neues Jahrb. Mineral., Monatsh.*, 289-294.

_____, BALEN, D., ŠĆAVNIČAR, S. & TIBLJAŠ, D. (1993): Zn-rich magnetoplumbite from Nežilovo, Macedonia. *Eur. J. Mineral.* **5**, 957-960.

BINNS, R.A., SCOTT, S.D., BOGDANOV, Y.A., LISITZIN, A.P., GORDEEV, V.V., GURVICH, E.G., FINLAYSON, E.J., BOYD, T., DOTTER, L.E., WHELLER, G.E. & MURAVYEV, K.G. (1993): Hydrothermal oxide and gold-rich deposits of Franklin seamount, western Woodlark Basin, Papua New Guinea. *Econ. Geol.* **88**, 2122-2153.

BOLTON, B.R., BOTH, R., EXON, N.F., HAMILTON, T.F., OSTWALD, J. & SMITH, J.D. (1988): Geochemistry and mineralogy of seafloor hydrothermal and hydrogenetic Mn oxide deposits from the Manus Basin and Bismarck Archipelago region of the southwest Pacific Ocean. *Marine Geol.* **85**, 65-87.

BONATTI, E. (1975): Metallogenesis at oceanic spreading centers. *Annu. Rev. Earth Planet. Sci.* **3**, 401-431.

_____, KRAMER, T. & RYDELL, H. (1972): Classification and genesis of sub-marine iron manganese deposits. *In* Ferromanganese Deposits on the Ocean Floor (D. Horn, ed). National Science Foundation, Washington, D.C. (146-165).

BOSTRÖM, K., RYDELL, H. & JOENSUU, O. (1979): Långban – an exhalative sedimentary deposit? *Econ. Geol.* **74**, 1002-1011.

BOYD, T. & SCOTT, S.D. (1999): Two-XRD-line ferrihydrite and Fe–Si–Mn oxyhydroxide mineralization from Franklin Seamount, western Woodlark Basin, Papua New Guinea. *Can. Mineral.* **37**, 973-990.

BROOKINS, D.G. (1989): Aqueous geochemistry of rare earth elements. *In* Geochemistry and Mineralogy of Rare Earth Elements (B.R. Lipin & G.A. McKay, eds). *Rev. Mineral.* **21**, 147-167.

BRUGGER, J. (1996): *The Fe, Mn, (V, Sb, As, Be, W) Deposits of Val Ferrera (Graubünden, Switzerland)*. Ph.D. thesis, Institute for Mineralogy and Petrography, Basel, Switzerland.

_____ & BERLEPSCH, P. (1996): Description and crystal structure of fianelite $Mn_2V(V,As)O_7•2H_2O$, a new mineral from Fianel, Val Ferrera, Graubünden, Switzerland. *Am. Mineral.* **81**, 1270-1276.

_____ & _____ (1997): Johninnesite $Na_2Mn^{2+}_9$ $(Mg,Mn)_7(AsO_4)_2(Si_6O_{17})_2(OH)_8$: a new occurrence in the Val Ferrera (Graubünden, Switzerland). *Schweiz. Mineral. Petrogr. Mitt.* **77**, 449- 455.

_____, BONIN, M., MEISSER, N., SCHENK, K., BERLEPSCH, P. & RAGU, A. (1999): Description and crystal structure of nabiasite $BaMn_9(VO_4)_6(OH)_2$, a new mineral from Central Pyrénées (France). *Eur. J. Mineral.* **11**, 879-890.

_____ & GIERÉ, R. (1999): As, Sb, and Ce enrichment in minerals from a metamorphosed Fe–Mn deposit, Val Ferrera, eastern Swiss Alps. *Can. Mineral.* **37**, 37-52.

_____, _____, GRAESER, S. & MEISSER, N. (1997): The crystal chemistry of roméite. *Contrib. Mineral. Petrol.* **127**, 136-146.

_____, _____, GROBÉTY, B. & USPENSKY, E. (1998): Scheelite–powellite and paraniite-(Y) from the Fe–Mn deposit at Fianel, Val Ferrera, eastern Swiss Alps). *Am. Mineral.* **83**, 1100-1110.

CORTESOGNO, L., LUCCHETTI, G. & PENCO, A.M. (1979): Le mineralizzazioni a manganese nei diaspri delle ofioliti liguri: mineralogia e genesi. *Rend. Soc. Ital. Mineral. Petrol.* **35**, 151-197.

COX, D.E., TAKEI, W.J., MILLER, R.C. & SHIRANE, G. (1962): A magnetic and neutron diffraction study of the Fe_2O_3–V_2O_3 system. *J. Phys. Chem. Solids* **23**, 863-874.

CRERAR, D.A., NAMSON, J., CHYI, M., WILLIAMS, L. & PENCO, A.M. (1982): Manganiferous cherts of the Franciscan assemblage. I. General geology, ancient and modern analogues, and implications for hydrothermal convection at oceanic spreading centers. *Econ. Geol.* **77**, 519-540.

DUNN, P.J. (1991): Rare minerals of the Kombat mine, Namibia. *Mineral. Rec.* **22**, 421-424.

_____ (1995): *Franklin and Sterling Hill, New Jersey: the World's Most Magnificent Mineral Deposits.* Privately published.

DZOMBAK, D.A. & MOREL, F.M.M. (1990): *Surface Complexation Modelling: Hydrous Ferric Oxide*. Wiley-Interscience, New York, N.Y.

ELDERFIELD, H. & GREAVES, M.J. (1982): The rare earth elements in seawater. *Nature* **296**, 214-219.

ESSENE, E.J. & PEACOR, D.R. (1987): Petedunnite ($CaZnSi_2O_6$), a new zinc clinopyroxene from Franklin, New Jersey, and phase equilibria for zincian pyroxenes. *Am. Mineral.* **72**, 157-166.

EVENSEN, N.M., HAMILTON, P.J. & O'NIONS, R.K. (1978): Rare-earth abundances in chondritic meteorites. *Geochim. Cosmochim. Acta* **42**, 1199-1212.

GAMBERI, F., MARANI, M. & SAVELLI, C. (1997): Tectonic, volcanic and hydrothermal features of a submarine portion of the Aeolian arc (Tyrrhenian Sea). *Marine Geol.* **140**, 167-181.

GEIGER, T. (1948): Manganerz in den Radiolariten Graubündens. *Beiträge zur Geologie der Schweiz, Geotechnische Serie* **27**.

GIERÉ, R. (1985): Metasedimente der Suretta-Decke am Ost- und Südostrand der Bergeller Intrusion: Lithostratigraphische Korrelation und Metamorphose. *Schweiz. Mineral. Petrogr. Mitt.* **65**, 57-78.

GOFFÉ, B. & OBERHÄNSLI, R. (1992): Ferro- and magnesio-carpholite in the "Bündnerschiefer" of the eastern Central Alps (Grisons and Engadine window). *Eur. J. Mineral.* **4**, 835-838.

GRAESER, S. (1995): Bergslagit aus den Schweizer Alpen. *Aufschluss* **46**, 15-22.

GRAMACCIOLI, C.M., GRIFFIN, W.L. & MOTTANA, A. (1982): Medaite, $Mn_6[VSi_5O_{18}(OH)]$, a new mineral and first example of vanadatopentasilicate ion. *Am. Mineral.* **67**, 85-89.

GRIGOR'YEV, N.A. (1967): Co-sedimentation of Be with Mn during the formation of rhodochrosite under hypergene conditions. *Dokl. Akad. Nauk SSSR* **173**, 1411-1413 (in Russ.).

GRÜNENFELDER, M. (1956): Petrographie des Roffnakristallins in Mittelbünden und seine Eisenvererzungen. *Beiträge zur Geologie der Schweiz, Geotechnische Serie* **18**.

GUILBERT, J.M. & PARK, C.F. (1986): *The Geology of Ore Deposits*. W.H. Freeman and Company, New York, N.Y.

HAAS, J.R., SHOCK, E.L. & SASSANI, D.C. (1995): Rare earth elements in hydrothermal systems: estimates of standard partial molal thermodynamic properties of aqueous complexes of the rare earth elements at high pressures and temperatures. *Geochim. Cosmochim. Acta* **59**, 4329-4350.

HARTE, B. (1987): Metasomatic events recorded in mantle xenoliths: an overview. *In* Mantle Xenoliths (P. H. Nixon, ed.). John Wiley & Sons Ltd., New York, N.Y. (626-640).

HEDENQUIST, J.W. (1983): *Waiotapu, New Zealand: The Geochemical Evolution and Mineralization of an Active Hydrothermal System*. Ph.D. thesis, Univ. of Auckland, Auckland, N.Z.

HEFLIK, W. (1989): Tilasite – quartz – laumontite association from a manganese deposit at Djebel Guettara, northern Algeria. *Bull. Polish Acad. Sci.* **37**, 93-101.

HEIN, J.R., YEH, H.W., GUNN, S.H., GIBBS, A.E. & WANG, C.H. (1994): Composition and origin of hydrothermal ironstones from central Pacific seamounts. *Geochim. Cosmochim. Acta* **58**, 179-189.

HEKINIAN, R., HOFFERT, M., LARQUÉ, P., CHEMINÉE, J.L., STOFFERS, P. & BIDEAU, D. (1993): Hydrothermal Fe and Si oxyhydroxide deposits from South Pacific intraplate volcanoes and east Pacific Rise axial and off-axial regions. *Econ. Geol.* **88**, 2099-2121.

HOLTSTAM, D., NYSTEN, P. & GATEDAL, K. (1998): Parageneses and compositional variations of Sb oxyminerals from Långban-type deposits in Varmland, Sweden. *Mineral. Mag.* **62**, 395-407.

HUEBNER, J.S., FLOHR, M.J.K. & GROSSMAN, J.N. (1992): Chemical fluxes and origin of a manganese carbonate – oxide – silicate deposit in bedded chert. *Chem. Geol.* **100**, 93-118.

HURFORD, A.J., FLYSCH, M. & JÄGER, E. (1989): Unraveling the thermo-tectonic evolution of the Alps: a contribution from fission track analysis and mica dating. *In* Alpine Tectonics (M. P. Coward, D. Dietrich & R. G. Park, eds.). *Geol. Soc., Spec. Publ.* **Xx**, 369-398.

IONOV, D.A., GRÉGOIRE, M. & PRIKHOD'KO, V.S. (1999): Feldspar – Ti-oxide metasomatism in off- cratonic continental and oceanic upper mantle. *Earth Planet. Sci. Lett.* **165**, 37-44.

KARPOV, G.A. & NABOKO, S.I. (1990): Metal contents of recent thermal waters, mineral precipitates and hydrothermal alteration in active geothermal fields, Kamchatka. *J. Geochem. Explor.* **36**, 57-71.

KATO, Y., OHTA, I., TSUNEMATSU, T., WATANABE, Y., ISOZAKI, Y., MARUYAMA, S. & IMAI, N. (1998): Rare earth element variations in mid-Archean banded iron formations: implications for the chemistry of ocean and continent and plate tectonics. *Geochim. Cosmochim. Acta* **62**, 3475-3497.

KIRCHHEIMER, F. (1959): Über radioaktive und uranhaltige Thermalsedimente, insbesonder von Baden-Baden. *Abh. Geol. L.-A. Baden-Württemberg* **3**, 1-59.

KLINKHAMMER, G.P., CHIN, C.S., WILSON, C. & GERMAN, C.R. (1995): Venting from the Mid-Atlantic Ridge at 37°17'N: the Lucky Strike hydrothermal site. *In* Hydrothermal Vents and Processes (L.M. Parson, C.L. Walker & D.R. Dixon, eds.). *Geol. Soc., Spec. Publ.* **87**, 87-96.

KNILL, M.D. (1996): The Pb–Zn–As–Tl–Ba-deposit at Lendenbach, Binn Valley, Switzerland. *Beiträge zur Geologie der Schweiz, Geotechnische Serie* **90**.

KRAUSKOPF, K.B. (1957): Separation of Mn from Fe in sedimentary processes. *Geochim. Cosmochim. Acta* **12**, 61-84.

LEHMANN, B., NAKAI, S.I.N., HÖHNDORF, A., BRINCKMANN, J., DULSKI, P., HEIN, U. & MASUDA, A. (1994): REE mineralization at Gakara, Burundi: evidence for anomalous upper mantle in the western Rift Valley. *Geochim. Cosmochim. Acta* **58**, 985-992.

LINIGER, M. (1992): *Der ostalpin-penninische Grenzbereich im Gebiet der nördlichen Margna-Decke (Graubünden, Schweiz)*. Ph.D. thesis, ETH, Zürich, Switzerland.

LIPIN, B.R. & MCKAY, G.A., eds. (1989): Geochemistry and Mineralogy of Rare Earth Elements. *Rev. Mineral.* **21**.

LIU, Y.-G., MIAH, M.R.U. & SCHMITT, R.A. (1988): Cerium: a chemical tracer for paleo-oceanic redox conditions. *Geochim. Cosmochim. Acta* **52**, 1361-1371.

MANCEAU, A. (1995): The mechanism of anion adsorption on iron oxides: evidence for the bonding of arsenate tetrahedra on free $Fe(O,OH)_6$ edges. *Geochim. Cosmochim. Acta* **59**, 3647-3653.

MANNING, B.A. & GOLDBERG, S. (1997): Adsorption and stability of arsenic(III) at the clay mineral–water interface. *Environ. Sci. Technol.* **31**, 2005-2011.

MARCHIG, V., GUNDLACH, H., MOLLER, P. & SCHLEY, F. (1982): Some geochemical indicators for discrimination between diagenetic and hydrothermal metalliferous sediments. *Marine Geol.* **50**, 241- 256.

MARQUER, D., CHALLANDES, N. & BAUDIN, T. (1996): Shear zone patterns and strain distribution at the scale of a Penninic nappe: the Suretta nappe (Eastern Swiss Alps). *J. Struct. Geol.* **18**, 753- 764.

_____, _____ & SCHALTEGGER, U. (1998): Early Permian magmatism in Briançonnais terranes: Truzzo granite and Roffna rhyolite (eastern Penninic nappes, Swiss and Italian Alps). *Schweiz. Mineral. Petrogr. Mitt.* **78**, 3, 397-414.

MARTIN-VERNIZZI, S. (1984): *La mine de Praborna (Val d'Aoste, Italie) : une série manganésifère métamorphisée dans le faciès éclogite.* Thèse de doctorat, Univ. Pierre et Marie Curie, Paris, France.

MASSONNE, H.J. & SCHREYER, W. (1987): Phengite geobarometry based on the limiting assemblage with K-feldspar, phlogopite, and quartz. *Contrib. Mineral. Petrol.* **96**, 212-224.

MOFFETT, J.W. (1990): Microbially mediated cerium oxidation in seawater. *Nature* **345**, 421-423.

MOORE, P.B., GUPTA, P.K.S. & LE PAGE, Y. (1991): The remarkable långbanite structure type: crystal structure, chemical crystallography, and relations to some other cation close-packed structures. *Am. Mineral.* **76**, 1408-1425.

NATHAN, Y. (1996): Mechanism of CO_3^{2-} substitution in carbonate-fluorapatite; evidence from FTIR spectroscopy, ^{13}C NMR, and quantum mechanical calculations; discussion and reply. *Am. Mineral.* **81**, 513-515.

NITSCH, K.H. (1970): Experimentelle Bestimung der oberen Stabilitätsgrenze von Stilpnomelan. *Fortschr. Mineral.* **47**(1), 48-49.

NUSSBAUM, C., MARQUER, D. & BIINO, G.G. (1998): Two subduction events in a polycyclic basement – Alpine and pre-Alpine high-pressure metamorphism in the Suretta nappe, Swiss Eastern Alps. *J. Metamorph. Geol.* **16**, 591-605.

NYSTEN, P. & ERICSSON, T. (1994): Fe-rich långbanite from the Nyberget ore-field, Sweden. *Neues Jahrbuch Mineral., Monatsh.*, 557-566.

OBERHÄNSLI, R. (1978): Chemische Untersuchungen an Glaukophan-führenden basischen Gesteinen aus den Bündnerschiefern Graubündens. *Schweiz. Mineral. Petrogr. Mitt.* **58**, 139-156.

OSTWALD, J. & NAYAK, V.K. (1993): Braunite mineralogy and paragenesis from the Kajlidongri mine, Madhya Pradesh, India. *Mineral. Deposita* **28**, 153-156.

PEARCY, E.C. & PETERSEN, U. (1990): Mineralogy, geochemistry and alteration of the Cherry Hill, California hot-spring gold deposit. *J. Geochem. Explor.* **36**, 143-169.

PERSEIL, E.A. (1991): La présence du Sb-rutile dans les concentrations manganésifères de St. Marcel – Praborna (Val d'Aoste – Italie). *Schweiz. Mineral. Petrogr. Mitt.* **71**, 341-348.

PFEIFER, H.-R., LAVANCHY, J.-C. & SERNEELS, V. (1991): Bulk chemical analysis of geological and industrial materials by X-ray fluorescence, recent developments and application to materials rich in iron oxide. *J. Trace Microprobe Techn.* **9**, 127-147.

_____, OBERHÄNSLI, H. & EPPRECHT, W. (1988): Geochemical evidences for a synsedimentary hydrothermal origin of Jurassic iron–manganese deposits at Gonzen (Sargans, Helvetic Alps, Switzerland). *Marine Geol.* **84**, 257-272.

PHILIPPOT, P. & SELVERSTONE, J. (1991): Trace-element-rich brines in eclogitic veins: implications for fluid composition and transport during subduction. *Contrib. Mineral. Petrol.* **106**, 417-430.

PUTNIS, A., FERNANDEZ-DIAZ, L. & PRIETO, M. (1992): Experimentally produced oscillatory zoning in the $(Ba,Sr)SO_4$ solid solution. *Nature* **358**, 743-745.

RAGU, A. (1990): *Pétrologie et minéralogie des minéralisations manganèsées métamorphiques dans le paléozoïque des Pyrénées Centrales*. Thèse de doctorat, Univ. Pierre et Marie Curie, Paris, France.

_____ (1994): Helvite from the French Pyrénées as evidence for granite-related hydrothermal activity. *Can. Mineral.* **32**, 111-120.

RICKWOOD, P.C. (1968): On recasting analyses of garnet into end-member molecules. *Contrib. Mineral. Petrol.* **18**, 175-198.

RÜCK, P. (1995): Stratigraphisch-sedimentologische Untersuchung der Schamser Decken. *Beiträge zur Geologischen Karte der Schweiz* **167**.

SCHAUFELBERGER, F.A. (1994): Arsenic minerals and their formation in hydrothermal systems. *In* Natural and Anthropogenic Geochemical Cycles of Arsenic (J. O. Nriagu, ed.). John Wiley & Sons, New York, N.Y. (403-415).

SCHMID, S.M., PFIFFNER, O.A. & SCHREURS, G. (1997): Rifting and collision in the Penninic zone of eastern Switzerland. *In* Deep Structure of the Swiss Alps – Results from NFP/PNR 20 (A. Pfiffner, ed.). Birkhäuser AG, Basel, Switzerland (160-185).

SCHREURS, G. (1995): Geometry and kinematics of the Schams nappes and adjacent tectonic units in the Penninic zone. *Beiträge zur Geologischen Karte der Schweiz* **167**.

SCHWERTMANN, U. & PFAB, G. (1994): Structural vanadium in synthetic goethite. *Geochim. Cosmochim. Acta* **58**, 4339-4352.

SCOTT, S.D. & BINNS, R.A. (1991): Hydrothermal processes and contrasting styles of mineralization in the western Woodlark and eastern Manus basins of the western Pacific.

In Hydrothermal Vents and Processes (L.M. Parson, C.L. Walker & D.R. Dixon, eds.). *Geol. Soc., Spec. Publ.* **87**, 191-205.

SERNEELS, V. (1993): Le Sidérolithique Suisse. *Minaria Helvetica* **13b**, 74-83.

SHANNON, R.D. (1976): Revised effective ionic radii and systematic studies of interatomic distances in halides and chalcogenides. *Acta Crystallogr.* **A32**, 751-767.

SORENSEN, S.S. & GROSSMAN, J.N. (1989): Enrichment of trace elements in garnet amphibolites from a paleosubduction zone: Catalina Schist, southern California. *Geochim. Cosmochim. Acta* **53**, 3155-3177.

STAATZ, M.H. & CARR, W.J. (1964): Geology and mineral deposits of the Thomas and Dugway ranges, Juab and Tooele counties, Utah. *U.S. Geol. Surv., Prof. Pap.* **415**.

STREIFF, V., JÄCKLI, H. & NEHER, J. (1976): Erläuterungen zum Blatt 1235 Andeer des Geologischen Atlas der Schweiz 1:2500. Atlasblatt 56. Schweizerische Geologische Kommission.

STUCKY, K. (1960): Die Eisen- und Manganerze in der Trias des Val Ferrera. *Beiträge zur Geologie der Schweiz, Geotechnische Serie* **37**.

TAYLOR, S.R. & MCLENNAN, F.S. (1985): *The Continental Crust: its Composition and Evolution*. Blackwell Sci. Publ., Oxford, U.K.

TRÜMPY, R. (1980): *Geology of Switzerland, a Guide Book.* **A**. *An Outline of the Geology of Switzerland*. Schweizerische geologische Kommission, Wepf, Basel, Switzerland.

VOCKE, R.V.J., HANSON, G.N. & GRÜNENFELDER, M. (1987): Rare earth element mobility in the Roffna Gneiss, Switzerland. *Contrib. Mineral. Petrol.* **95**, 145-154.

VON BLANCKENBURG, F. (1992): Combined high-precision chronometry and geochemical tracing using accessory minerals applied to the central-Alpine Bergell intrusion (central Europe). *Chem. Geol.* **100**, 19-40.

WHITE, D.E. (1974): Diverse origins of hydrothermal ore fluids. *Econ. Geol.* **69**, 954-973.

APPENDIX: METHODS OF INVESTIGATION

Petrographic studies have been carried out on standard polished sections 30 μm thick. Because of the generally small grain-size and complex mineral associations in the ores, we used a methodological approach that included transmission and reflection optical microscopy, cathodoluminescence (Technosyn Cold Cathode Luminescence Model MkII, operated at 25 kV and 100 μA), and electron microscopy in both secondary electron (SE) and back-scattered electron (BSE) modes. Cathodoluminescence (CL) has proven to be a very powerful method for easily finding strontian barite (yellow), fluorapatite (yellow to green), barylite (blue), bergslagite (pale blue), and an yttrium phosphate (bright blue). CL further revealed zoning in fluorapatite, barite, and carbonates.

Quantitative chemical analyses of minerals were carried out with a JEOL JXA–8600 electron microprobe at the Institute for Mineralogy and Petrography, University of Basel, Switzerland, with analytical conditions and standards similar to those used by Brugger & Gieré (1999). Geochemical analyses of major and some trace elements were made of 59 whole-rock samples by X-ray fluorescence (XRF) at the University of Lausanne, Switzerland, following the procedure of Pfeifer *et al.* (1991). Inorganic CO_2 was determined by coulometric titration, using N_2 as a carrier gas. Analyses of five different whole-rock samples were repeated using O_2-rich gas to oxidize the "organic" carbon (present as graphite) in the sample, and yielded the same CO_2 content within analytical error. Concentrations of an extended set of trace elements were measured by inductively coupled plasma – mass spectrometry (ICP–MS) at Service d'Analyse des Roches du CNRS, Nancy, France on 20 samples previously analyzed by XRF.